

DOPAMINE DETECTION VIA SURFACE ENHANCED RAMAN SCATTERING  
FOR PARKINSON'S DISEASE

by

Eric Gerard Cutler

A thesis submitted to the faculty of  
The University of North Carolina at Charlotte  
in partial fulfillment of the requirements  
for the degree of Master of Science in  
Mechanical Engineering

Charlotte

2019

Approved by:

---

Dr. Hansang Cho

---

Dr. Kirill Afonin

---

Dr. Yong Zhang

---

Dr. Tsing-Hua Her

©2019  
Eric Cutler  
ALL RIGHTS RESERVED

## ABSTRACT

ERIC CUTLER. Dopamine Detection for Parkinson's Disease Via SERS Plasmonic Enhancement. (Under the direction of DR. HANSANG CHO)

Motion is controlled via the excitatory or inhibitory responses of the motor pathway by receptors in Substantia Nigra of the brain, modulated by a main neurotransmitter dopamine (DA). Parkinson's Disease (PD) is the neurological disorder effecting many attributes resulting from brain tissue damage, with the main impact on the human kinetic behavior and estimated statistics of patients with PD at 7-10 million people worldwide. PD occurs when misfolded protein  $\alpha$ -synuclein aggregates destroy the neuron cells at their synapse, where they disrupt the DA pathway from neuron to neuron, thus resulting in depletion of the DA the cellular communication system. The degree of PD can be monitored by focusing on DA levels, this goal requires a biofriendly scheme with high sensitivity and specificity design features. Here we present a nanoprobe utilizing the design for PD recognition by a DNA aptamer stem loop that will recognize small specific regions of the DA via a specific nucleotide complementary sequence. The DNA is sequenced with thiol that covalently bonds to gold nanoparticles (GNPs) coated with tannic acid. GNPs perform a plasmonic enhancement capable of  $10^{10}$  signal increase. The gold operates as a plasmonic enhancer to increase the response signaling of the probe. When a DA molecule is within proximity of the nanoprobe, the DNA binds the DA to the probe to create a signal change. The signal itself is a Raman Spectra induced laser that measures emission frequencies of the targeted area. Validation of probe components was indicated by Dark Field for GNP immobilization onto platform with  $7\text{mm}^2$  surface area with homogeneous or aggregated (by  $\text{CuSO}_4$ ) plasmonic effect, gel electrophoresis for bioreceptor DNA

bonding to biotarget DA, and fluorescence Well Plate for DNA coupling to GNP. The two main SERS elements are GNPs and DA, SERS of GNPs demonstrated a broad band between  $1200\text{-}1700\text{cm}^{-1}$  with a sharp band inside between  $1500\text{-}1700\text{cm}^{-1}$  while SERS of DA shows target peaks at  $1287\text{cm}^{-1}$ ,  $1456\text{cm}^{-1}$  and  $1611\text{cm}^{-1}$ . Expected sensitivity illustrates a limit of detection (LOD) of DA at  $0.75\text{nM}$  with a linear range (LR) corresponding toward high accuracy range of signal output and DA concentration changes at  $1\text{nM}\text{-}1\mu\text{M}$ . Expected selectivity illustrates the probe bioreceptor can distinguish between similar DA molecules norepinephrine and tyrosine, two molecules present with DA in brain tissue or patient samples, with an average higher binding rate toward DA. In conclusion, the nanoprobe utilizes a DNA aptamer as a bioreceptor and a gold nanoparticle (GNP) for signal enhancement. producing a SERS plasmonic enhancement  $10^{10}$  fold. Results indicate nanoprobe sensitivity is expected to relay a linear range of  $1\text{nM}\text{-}1\mu\text{M}$  with a limit of detection at  $0.75\text{nM}$  while selectivity of probe is expected to relay stronger bonding toward DA against similar structured molecules. Future plans include *in vitro* neuron chip coated with PD neurons and DA-probe to measure DA levels for neuron-neuron communication.

## ACKNOWLEDGMENTS

I would like to express my sincere gratitude and give special acknowledgement to my research advisor Dr Hansang Cho. His guidance and hard work in affiliation with my research, along with his recommendations have helped me with significantly. His support has helped with experimental design, research presentation, and experimental analysis. Without his supervision, this project would not have happened. Furthermore, I would like to extend my sincere gratitude toward other supporting members for this project. Dr. Afonin for his support in biochemistry, his support and lab member Justin Halman helped improve experimental designs with DNA. Dr. Her for his support in gold nanoparticle analysis, his support helped assess conditions with gold nanoparticles. Dr. Zhang and his lab member Jose Castaneda for support in microscope SERS readout, their support greatly helped readout assessments. Dr. Kang for her support in nanoparticle assessment, she helped significantly helped with project optimization.

## TABLE OF CONTENTS

LIST OF TABLES .....	vii
LIST OF FIGURES .....	viii
LIST OF ABBREVIATIONS.....	x
CHAPTER 1: INTRODUCTION.....	1
1.1 Neurological Disease: .....	1
1.2 Nanoprobes: .....	5
1.3 SERS Signaling:.....	7
CHAPTER 2: SCHEMATIC AND DESIGN.....	10
2.1 Dopamine Probe Requirements and Parameters: .....	10
2.2 Probe and Platform Schematic: .....	12
2.3 DNA-DA Binding Sites: .....	14
2.4 DNA Coupling to GNP Thiol Groups:.....	17
2.5 GNP Plasmonics and Size:.....	17
2.6 Fabrication and Essay Design: .....	19
2.7 Platform and Probe Verification: .....	22
2.8 Platform Material List: .....	31
CHAPTER 3: RESULTS AND DISCUSSIONS .....	33
3.1 Dopamine Nanoprobe: .....	33
3.2 Raman Spectra of Components:.....	34
3.3 Dopamine Nanoprobe Detection:.....	35
CONCLUSION.....	42
REFERENCES .....	43
APPENDIX.....	45

## LIST OF TABLES

TABLE 1: Urine DA samples of various age groups for healthy and PD percentages	10
TABLE 2: Plasma DA conditions for various healthy and PD percentage conditions	11
TABLE 3: Sequences for RNA and DNA containing DA binding motifs	15

## LIST OF FIGURES

FIGURE 1: Intracellular effect of Parkinson Disease.	4
FIGURE 2: PD schematic for cellular pathway induced by $\alpha$ -synuclein.	5
FIGURE 3: Plasmonic effect of gold nanoparticles.	8
FIGURE 4: DA nanoprobe three stage schematic for DA SERS readout. (A) GNP are aggregated together, (B) followed by coating of DNA strands for DA, and (C) finalized with SERS readout of Probe.	13
FIGURE 5: Dopamine chemical structure and DNA sequence with complementary (red) and invariant (blue) nucleotides for DNA binding to DA and stem loop exergonic stability.	16
FIGURE 6: DNA aptamer (A) gel electrophoresis test for DNA folding stability at different temperatures, and (B) UV-melting temperature plot for DNA.	16
FIGURE 7: Gold nanoparticle plasmonic resonances at Various Diameters	18
FIGURE 8: 60nm Diameter GNP with induced electric field 1V/m in the EzKx direction, and the plasmonic response at various wavelengths	19
FIGURE 9: 60nm Diameter GNP induced with a 1V/m Electric field for the response (A) at its surface and adjacent toward its surface, and (B) the peak electric field (V/m) pattern for various wavelengths of the two locations.	19
FIGURE 10: Platform and DA-probe fabrication from (1) APS coating onto glass, (2) PDMS bonding to glass slide, (3) GNP insertion and (4) DNA insertion.	21
FIGURE 11: SERS application of a DA-probe measurement.	22
FIGURE 12: APS coating validation by water droplet test. (A) Statistical assessment between hydrophobic or hydrophobicity of glass cleaned and with or without APS, and (B) droplet angle assessment.	23
FIGURE 13: GNP immobilization observed at (A) zero, left, and one wash, right, and (B) two times wash, left, and 3 times wash, right (scale bar 200 $\mu$ m).	25
FIGURE 14: GNP aggregation induced by CuSO <sub>4</sub> (scale bar 200 $\mu$ m).	25

- FIGURE 15: Plasma treatment level optimization (A) at three different power levels and (B) their corresponding effect on GNP coating with APS and GNP leakage through PDMS (scale bar 200 $\mu$ m). 27
- FIGURE 16: TEMRA dye attached to DNA fluorescence signals. (B) DNA-FL concentration differences and corresponding GNP binding capabilities, and (C) DNA-FL DTT removal validation. 30
- FIGURE 17: DNA bonding with DA-FL by a gel electrophoresis essay 31
- FIGURE 18: Raman spectra's of (A) GNP and its (B) visual fluorescence image, (C) Raman spectra's of DNA and its (D) visual fluorescence image, and (E) Raman spectra's of dopamine and its (F) visual fluorescence image. 35
- FIGURE 19: (A) SERS Calibration with probe components, (B) enhanced for glass and DA Raman spectra, and (C) comparison between DA and GNP spectra. 36
- FIGURE 20: Detection of 1mM DA with GNP-DNA-DA probe at (A) low aggregation, (B) compared with GNP-DNA reference, and (C) compared with DA reference. 38
- FIGURE 21: Detection of 1mM DA with GNP-DNA-DA probe at (A) high aggregation, (B) compared with GNP-DNA reference, and (C) compared with DA reference. 39
- FIGURE 22: (A) GNP-DNA-DA cluster before and after activation of SERS (10% power). (B) SERS response from first iteration of SERS and second iteration of SERS. 40
- FIGURE 23: SERS calibration of (A) DA and (B) GNP 41

## LIST OF ABBREVIATIONS

APS	3-Aminopropyl triethoxysilane
DNA	deoxyribonucleic acid
DNA-FL	deoxyribonucleic acid bonded with TEMRA dye
DA	Dopamine
GNP	Gold nanoparticle
PD	Parkinson's Disease
PDMS	Polydimethylsiloxane
SERS	Surface Enhanced Raman Spectroscopy

## CHAPTER 1: INTRODUCTION

### 1.1 Neurological Disease:

There are approximately 100 billion neurons in the human brain that depend on physical arrangement and biochemical operation of neurons for proper brain functionality. The biochemical sub group of neuron communication for transporting bio-messages throughout the body are defined as neurotransmitters with specific goal-oriented pathways. The kinetic and dynamic behavior of the human body depends on the quick communication between neurons utilizing a neurotransmitter known as dopamine (DA) to cause excitatory or inhibitory responses along the motor pathway by (additionally, dopamine participates in other applications of neuronal communication and command within various regions of the brain for other functions of the body, such as mood enhancers). Specifically, the dynamics of the motor system for muscle control is controlled within a region of the brain associated as the Basal Ganglia. The Basal Ganglia is composed of smaller brain tissue regions each with its own designated task. They operate from stimulation of inputs from their corresponding cortical area or send outputs for their corresponding cortical area by processing immense amounts of information. One of these regions is known as the Substantia Nigra, which is part of the indirect and direct modulation of neuron pathway for muscle regulation. Here, the neurotransmitter dopamine is created by cells in the par's compacta of the Substantia Nigra, where upon production, are released through a pathway that begins within the striatum. The striatum acts as an introduction from a single path into two available paths, the indirect and direct pathways. If dopamine is sent through the direct pathway, an excitatory effect occurs where an increase in motor activity is activated by the D1 receptors. However, in the event too much excitation is activated from dopamine, the

neurotransmitter cholinergic is sent along the indirect pathway for an inhibitory effect on motor activity. Dopamine can also be sent along the indirect pathway to turn down the indirect pathway if cholinergic surpassed the desired motor activity response. Any damage to this complex circuitry, such as neuron death, can lead to unregulated motor responses. As damage increases, the motor responses become increasingly unstable [Ref 1]

Parkinson's disease (PD) occurs in patients when damage of neurons interferes with the neuron to neuron biochemical communication of DA, more specifically, at a DA depletion of 70-75% from normal conditions. The damage results in hypokinetic, a muscle contraction symptom causing reduced movement, rigidity, tremors, and poor reflexes of the muscular system. Without proper dopamine transport, the neuronal communication breaks down. Patients associated with PD also develop damage to the sympathetic nervous system from a loss of the neurotransmitter norepinephrine (NE). Norepinephrine is a final transition from dopamine along the nervous system pathway that never reaches its state if there isn't enough dopamine present to transition into norepinephrine. The lack of proper norepinephrine concentration can lead into a loss of nerve endings, thus causing more issues for patients with Parkinson's disease [Ref 2].

Worldwide incidence estimates of PD can range from 5 to 35 or even greater than 35 new cases per 100,000 individuals yearly, making it the second or third (depending on demographics) neurological disease diagnosed each year. In terms of probability, PD is rare before 50 years of age, but the incidence increases 5 to 10-fold from the sixth to the ninth decade of life. Mortality is not increased in the first decade after disease onset, but increases thereafter, eventually doubling compared with the general population. This eludes to increased sensitivity per diagnostics as PD condition progresses. However,

early diagnostics is difficult to achieve due to measurement limitations and overlapping features of PD with other neurological diseases at early stages. Additionally, PD in gender is twice as common in men as in women [Ref 3]. From three years after initial diagnostics of PD, DA loss increases significantly, by ten years, DA producing cells show a 30-60% loss [Ref 4].

While PD is a direct result of DA depletion, the catalyst causing the effect is associated with an intracellular protein called  $\alpha$ -synuclein.  $\alpha$ -synuclein and DA possess a synergetic relationship in healthy and unhealthy conditions. Normally,  $\alpha$ -synuclein acts as a protein near the neuron synapse that helps in the diffusion of dopamine vesicles for dopamine transport to the synaptic connected neuron. However, in unhealthy conditions, a misfolded  $\alpha$ -synuclein aggregates into an assembly of toxic oligomeric species causing internal neuronal damage at various cellular key regions [Ref 5].

In healthy conditions, the excitatory DA is synthesized inside the brain after its precursor L-DOPA passes through the blood brain barrier. L-DOPA, converted from tyrosine by tyrosine hydroxylase, is converted to dopamine by aromatic amino acid decarboxylase. From here, dopamine is passed from neuron to neuron until it reaches the stage to become norepinephrine [Ref 6]. Dopamine maintains its synaptic passage by traveling down the neuron axon from transport proteins like tau, where upon reaching the synapse, a v-SNAPE protein absorbs the DA to incase it in a multimeric membrane-bound  $\alpha$ -synuclein forming a N-C chain. From here, a t-SNARE protein bonded with  $\alpha$ -synuclein and SNAP 25 protein pulls the vesicle toward the synapse membrane for diffusion, where the dopamine is released into the synaptic cleft (recycling can occur picking up left over dopamine for reuse). However, in unhealthy patients with PD, the  $\alpha$ -synuclein burdens the

vesicle membrane, preventing the v-SNARE from releasing or absorbing the DA, thus trapping the DA inside. Additionally, the misfolded  $\alpha$ -synuclein prevents the t-SNARE and SNAP 25 from interacting with the vesicle to defuse the DA. From here, an input of DA continues and delivered down the axon toward the synapse. This results in a clogging effect causing intracellular neuronal damage. Figure 1 illustrates the intracellular effect.

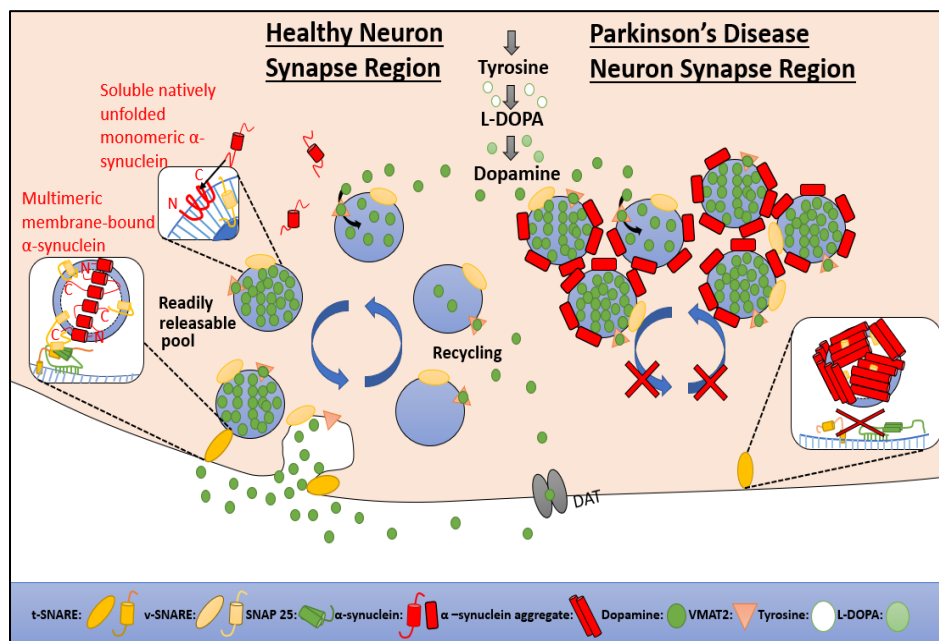


FIGURE 1: Intracellular effect of Parkinson Disease.

As the misfolded  $\alpha$ -synuclein propagates, it spreads throughout the entire cell. This includes  $\alpha$ -synuclein aggregations at the ER system and Mitochondrial, where pathways such as  $\alpha$ -synuclein Proteostasis, mitochondrial function, oxidative stress, calcium homeostasis, axonal transport and neuroinflammation are formed. Ideally, the misfolded proteins are cleaned up by the Ubiquitin-proteasome system and the macroautophagic system, however, as the aggregation spreads, toxic oligomers create the mitochondrial dysfunction that induces perturbed  $\alpha$ -synuclein Proteostasis cycle to further help the

misfolded proteins, thus leading toward oxidative and neural inflammation. Each of these conditions further disrupts the dopamine transport, further preventing any fix at the synaptic disruption. This leads to a system breakdown where the neuron dies and the  $\alpha$ -synuclein spreads unto other neurons. Figure 2 illustrates this cellular schematic. As the damage of the cells increase, do Lewy Bodies (clumps of brain proteins) develop in Parkinson's disease patients. Because of this, misfolded  $\alpha$ -synuclein or dopamine depletion form a definitive diagnosis for idiopathic PD conditions [Ref 7, 8].

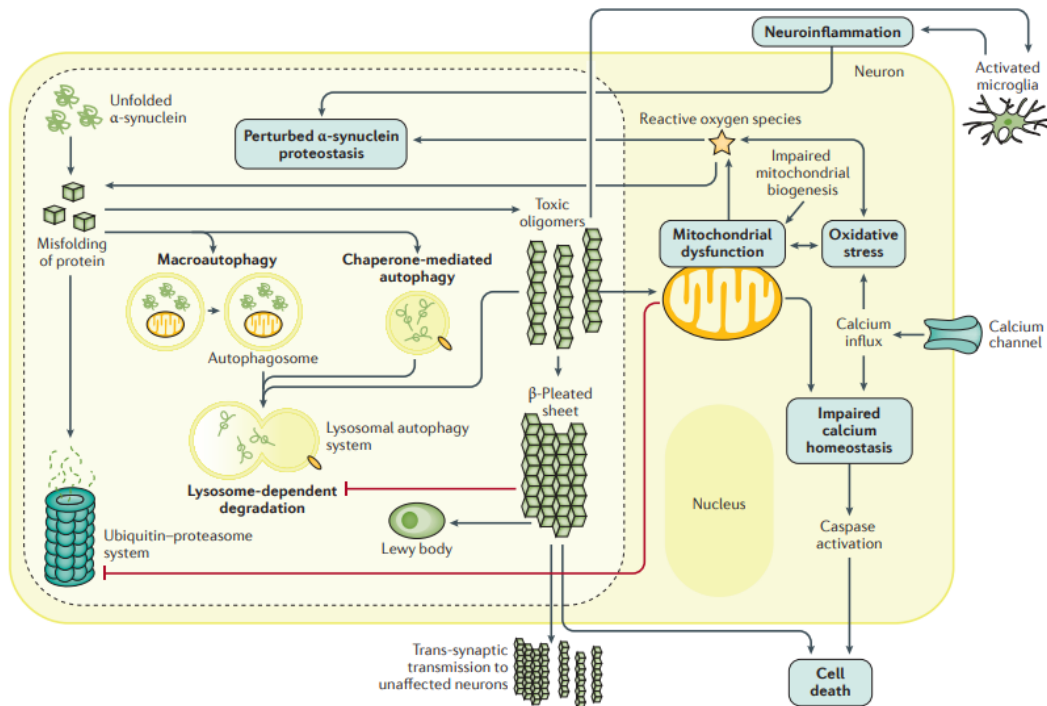


FIGURE 2: PD schematic for cellular pathway induced by  $\alpha$ -synuclein.

## 1.2 Nanoprobes:

Nanoprobes are nanoscale sensors designed with careful consideration for in the fields of chemistry, physics, biomaterial, microfluidics, thermodynamics, and bioengineering for motivation to achieve desired detection and monitoring of a target molecule. This requires

specific aims of the design to achieve the functionality where the nanoprobe can adjust its emitted signal as target molecules leaves or enters the parameter area that can induce conformational changes. The signal quality will correlate toward the sensitivity and selectivity of the probe, where sensitivity represents low detectable concentrations of a volumetric region, and selectivity details the emphasis on target molecule with neglect of other molecules within the volumetric region. Nanosensors have two main components toward their design, a bioreceptor and a measurement type. The bioreceptor represents the nanoprobe component that can register and bond with a target molecule, whether be a protein or oligonucleotide. A target molecule possesses unique bonding sites, making their recognition complex. Furthermore, a once bound, the bioreceptor must be able to equate efficient bonding energy to maintain the bonding. There exist different types of bioreceptors in protein or DNA form. Once the bioreceptor has completed its task, the probe measurement component must be able to relay the response with a signal and an equipment type must be able to evaluate the information for a measurement assessment. This comes either in an induced, absorbed, emitted signaling process, or a self-induced signaling process. There exist many types of the design, however, the selected one must contribute efficient sensitivity and selectivity with biofriendly features.

Current dopamine detection probes suffer from three main categories; the inability to exhibit a strong enough signal that can penetrate the deep biological barriers of a brain sample, the optimization for simultaneous high signal emission without emitting toxicity into the natural environment sample and preventing false positive signaling brought on by similar molecules. Probe development up to date have required a sacrifice in either signal strength or toxicity effect. The standards for increasing the strength, such as

electrochemical or quantum dots, possess a strong signal with good sensitivity, but produce damage to the cells. This makes these types of probes good for only dopamine detection from patient urine or plasma samples but limits their possible for Parkinson's disease models with *in vivo* or *ex vivo* studies [Ref 9, 10]. Another issue that arises, is the similarity between certain molecules with dopamine, especially norepinephrine [REF]. Some probes suffer from the ability to emit confident signaling due to concerns that the biological recognition component may acquire the wrong molecule [REF]. In this thesis, a Raman scattering signal is used as the measurement type to measure DA, and a DNA strand is used as the bioreceptor to bond with DA.

### 1.3 SERS Signaling:

When light is irradiated on molecules from a nanoprobe substance, the light is absorbed and scattered by the molecules as they release the vibrational energy that increased their kinetic energy status. While the induced light and the emitted light share a near equal wavelength pattern, slight differences occur related to the molecule composition, this phenomenon where the light is scattered with frequency change is called Raman scattering. Because this frequency variation is specific to molecular vibration, it is possible to analyze composition of material by analyzing spectrum of Raman scattered light. Here, Raman scattered light contains various fingerprint information on DA, along with the probe it's attached too [Ref 12]. The Raman signal can be enhanced by developing a plasmonic source near the molecule substance and nanoprobe surface, commonly selected as metallic. The plasmonic effect occurs when the electron surface of a metallic structure is excited with high energy. The electrons vibrate at high kinetic energies that form a highly heated source known as a plasmon hot spot. When an electromagnetic source is induced upon the

metallic structure, the signal is absorbed, then emitted with amplified electromagnetic field intensity due to the plasmon field passing on its excited energy source. Depending on the metal type, and geometry, each wavelength produces a change in peak electromagnetic intensities, with a single or multiple peak electromagnetic field associate with specific wavelengths corresponding to plasmon modes. The plasmon associated with these wavelengths are known as surface plasmon resonance. Amplification factors from surface plasmon resonance can reach folds up to  $10^{10}$  [Ref 13]. Additionally, gaps between two metallic particles can induced a plasmon gap resonance that further amplifies the signal, Figure 3 illustrates the plasmonic effect of gold nanoparticles. Surface Enhanced Raman Spectroscopy (SERS) is a technique that incorporates the plasmonic enhancement effect of metal and gap for enhancement factors up to  $10^{14}$  [Ref 14]

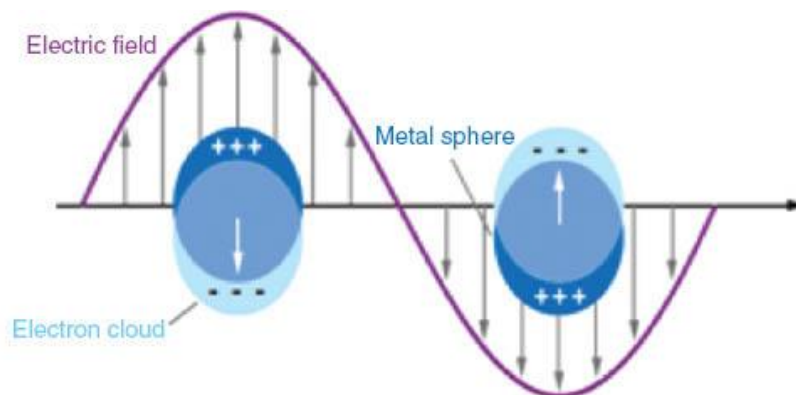


FIGURE 3: Plasmonic effect of gold nanoparticles.

Here we propose a nanosensor that takes advantage of chemistry, biology, and mechanical engineering traits to create a more reliable nanoprobe with a simplistic design, improved sensitivity signal output, all within the limits of bio-capability for potential cellular application. The biology component in the design consists of synthetic antibodies known as aptamers that operate as “grabbers” for the target molecule. These biological components operate as synthetic anti bodies that can maintain biological recognition in

combination with customizable configuration. This flexibility reduces the necessity for complexity. The mechanical engineering and biomaterial contribute applies through material and structural aspects for electromagnetic radiation control that enables surface plasmonic enhancement and aptamer configuration control. The chemistry consists of a buffer for pH stabilization, coupling the DNA to the probe, and immobilization of the probe to the platform surface. The probe will detect dopamine concentrations utilizing the traits mentioned above for an enhance Raman signal detailing concentration levels and changes based on the laser emission spectra. The dopamine concentrations will be observed for two purposes. One purpose will function as dopamine deviation from homeostasis level test for Parkinson's Disease detection module. The second purpose will represent monitoring dopamine fluctuations and dynamics within a Parkinson's Disease *in vitro* brain model. The first will serve as the primary project goal while the second purpose will be evaluated in future experiments.

## CHAPTER 2: SCHEMATIC AND DESIGN

## 2.1 Dopamine Probe Requirements and Parameters:

A nanosensor for dopamine detection requires high sensitivity, proper selectivity, and stability. Dopamine in the Substantia Nigra possesses low concentrations relative toward the rest of the brain. However, during PD initial stages, small percentages representing DA reduction must be able to be detected. DA measurements are commonly conducted by either a urine test, Table 1 or plasma test, Table 2. At 10% DA reduction, PD can be monitored for conditional changes after 4 years of diagnose, which requires sensitivity detection levels near 30-50nM for urine and above 6.5pM for plasma. At 0.1% DA reduction, PD can be monitored for conditional changes for initial PD development (before common PD diagnostics), which requires sensitive detection levels near 50-500pM for urine and above 0.065pM for plasma. The extremely low conditions make early PD difficult to detect.

TABLE 1: Urine DA samples of various age groups for healthy and PD percentages

Age	Healthy		10% DA Reduction		0.1% DA Reduction	
	Conventional Units ( $\mu\text{g}/24\text{h}$ )	SI units (nmol/24h)	Conventional Units ( $\mu\text{g}/24\text{h}$ )	SI units (nmol/24h)	Conventional Units ( $\mu\text{g}/24\text{h}$ )	SI units (nmol/24h)
3-8 yr	80-378	523-2472	8-37.8	52.3-247.2	0.08-0.378	0.523-2.472
9-12 yr	51-474	334-3100	5.1-47.4	33.4-310.0	0.051-0.474	0.334-3.100
13-17 yr	51-645	334-4218	5.1-64.5	33.4-421.8	0.051-0.645	0.334-4.218
>17 yr	52-480	340-3139	5.2-48.0	34.0-313.9	0.052-0.480	0.340-3.139

TABLE 2: Plasma DA conditions for various healthy and PD percentage conditions

Type	Healthy		10% DA Reduction		1% DA Reduction	
	Conventional Units (ng/L)	SI units (nmol/L)	Conventional Units ( $\mu\text{g}/24\text{h}$ )	SI units (nmol/24h)	Conventional Units ( $\mu\text{g}/24\text{h}$ )	SI units (nmol/24h)
Supine adult	<10	<0.065	<1.0	<0.0065	<0.010	<0.000065
Ambulatory adult	<20	<0.13	<2.0	<0.013	<0.020	<0.00013
3-15 yr	<60	0.39	<6.0	<0.039	<0.060	<0.00039

This means DA-nanoprobe readout within realm of possibility should achieve concentration sensitivity somewhere between high pM to low nM. The lowest value represents what is known as the Limit of Detection (LOD). The LOD presents the possibility that when a solution containing DA is transferred from point A to point B, whether by patient sample going through an inlet to exit channel on a chip, or a dopaminergic neuron passing DA at the synapse to another dopaminergic neuron, slight deviations can be noticed. The accuracy of those recordings depending on the Linear Range (LR) capabilities of the nanosensor. As the surrounding media and environment presents complexity that interferes with nanoprobe stability and readouts, combined with the fact low concentration of target molecules are difficult for a single to lock onto a target at larger distances, the LR details what range of low concentration the probe exhibits a corresponding linear signal output. This range (and any concentration above) informs of probe high accuracy probability, the gap between the LOD and lower boundary of LR details a region where the probe becomes less accuracy, but can still achieve a signal readout for detection, and the range below the LOD shows unachievable detection. For proper DA detection, a LR pertaining toward low nM to low  $\mu\text{M}$  is desired.

Because nanoprobe are comprised of multiple components (a bioreceptor, base, enhancement factor component, etc.), their stability requires each of these elements can remain coupled together without interference in their desired structure and operation. DA itself is a small molecule, this requires a bioreceptor that is capable of possessing binding sites pertaining toward the small size. Additionally, the environment is under constant interference forces such as movement, this requires the bioreceptor to maintain bonding upon competing or interrupting forces. Signal enhancement elements generally utilize energy transfer, this produces an increase in localized heat or electric fields, these conditions can interrupt the structure of the bioreceptor coupled to the probe. Further requiring the bioreceptor to maintain stability upon induced energy events.

Dopamine itself possesses a complex pathway with molecules of similar structures. From tyrosine to L-DOPA before dopamine, and epinephrine (or norepinephrine) after dopamine, the whole pathway of neurotransmitters each contain the similar elements that could theoretically interfere with the probe bioreceptor. The two most capable are tyrosine and epinephrine. These eludes to the potential for false positive signaling, that is, a response showing higher or lower detection values of DA than what is present, otherwise known as false positive signaling. Because of this, the nanosensor must be able to differentiate between DA and other similar molecules.

## 2.2 Probe and Platform Schematic:

Here, we developed a nanosensor for DA detection that utilizes a three-stage operation with label free identification and plasmonic enhancement. The probe itself is comprised of a gold nanoparticle (GNP) coated with tannic acid for stability acts as the base and plasmonic signal enhancer for the nanoprobe. A DNA aptamer sequenced with

two stem loops that are sequenced with DA bonding arrangement is selected as the bioreceptor. Together, they form a nanoprobe that can bond to DA, and enhance a Raman signal for DA readout. Probe design begins in Stage 1 with induced GNP self-aggregation to form randomized homogenous small clusters by electrostatic forces. Stage 2 is conducted by coating the GNPs with the DNA bioreceptor by sequencing a thiol group to the edge of the DNA. After Stage 2, DA will be brought within close proximity of the GNP surface. In Stage 3, an induced laser signal is absorbed by the probe GNP-DNA-DA components, where the plasmonic effect occurs energizing the probe, which enhances the emission signal for a SERS readout. Figure 4 illustrates the DA nanoprobe schematic. The size of the GNP was selected at 60nm, as the value is within range for maximum plasmonic enhancement and surface area coverage while still remaining small enough for biological impact, such as cellular uptake.

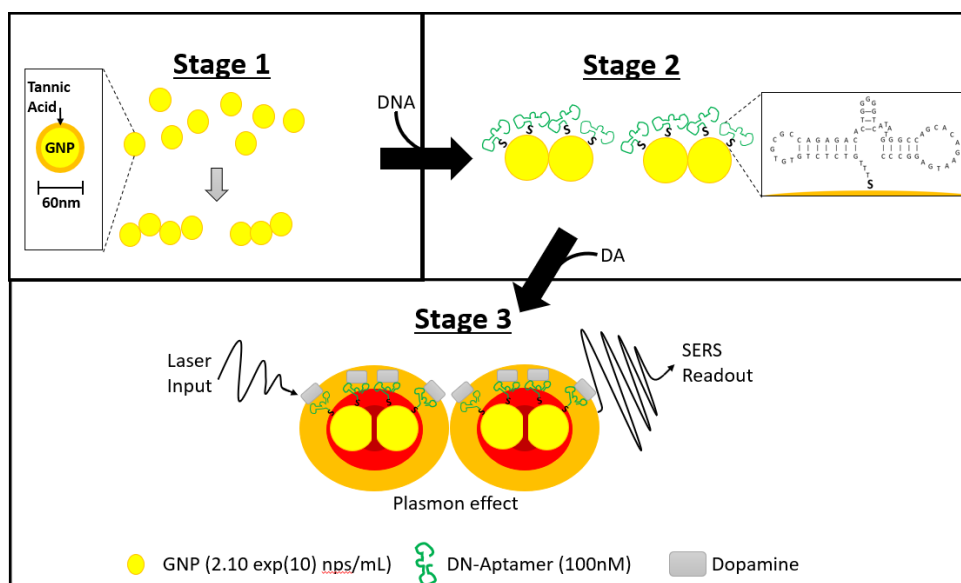


FIGURE 4: DA nanoprobe three stage schematic for DA SERS readout. (A) GNP are aggregated together, (B) followed by coating of DNA strands for DA, and (C) finalized with SERS readout of Probe.

A platform was constructed to secure the nanoprobe assays. The platform consists of a multi-well chip with a 3mm diameter for each hole and thickness of 2mm. Material of chip is made from a transparent polymer called Polydimethylsiloxane (PDMS). PDMS is a polymer that offers easy fabrication with high tolerance mechanical properties. The PDMS is coupled with a glass slide coated with 3-Aminopropyl triethoxysilane (APS) to form the bottom of the wells, where the APS creates a strong electrostatic bonding for the GNPs for immobilization. Each well contains a volume of  $14.137\text{mm}^3$  with a surface area of  $7.07\text{mm}^2$ . Figure 10 shows the chip design.

### 2.3 DNA-DA Binding Sites:

The DNA aptamer was converted from an RNA DA strand by a deoxy version of the same sequence functional homolog. During conversion, the hydroxyl in the 2' position of the RNA was removed for increased stability. Table 1 shows the RNA and DNA sequences for DA. The DNA strand consist of two stem loop regions connected by a smaller stem loop. The side stem loops represent the binding domain for DA with five complementary bases (T-G-T-G-C) and two invariant bases (G-C) for one of the stem loop motif and five complementary bases (G-C-A-C-A) and three invariant bases (A, G-A) for the other stem loop motif. The DNA structure is highly dependent on Watson & Crick base pairing along the loops for motif stability of the tertiary structure. The precise arrangement of the two invariant nucleotides in on stem loop and three in the other stem loop are primarily responsible to the binding affinity and specificity toward DA. The complementary bases offer further support for the binding affinity and specificity. Observed dissociation constant was found to be at  $0.7 K_d (\mu\text{M})$  []. DA itself is monoamine compound with positive inotropic activity of the chemical structure  $\text{C}_8\text{H}_{11}\text{NO}_2$  where two

hydroxide elements form on one end, forming the binding sites of the DA where the DNA will attach onto. Figure 5 illustrates the DNA aptamer secondary structure and its binding sites for DA. Additionally, a gel electrophoresis on a Native 8% gel and UV absorbance was conducted to show the folding structure of the DNA, where the temperature shows stability between 25-47°C at bands of 30kDA, Figure 6A. Furthermore, a melting temperature plot shows the peak is represented of the largest change in DNA structure at 75°C where the DNA is unfolded, that is, the melting temperature at which half of the hydrogen bonds of the DNA aptamer are dissociated, Figure 6B.

TABLE 3: Sequences for RNA and DNA containing DA binding motifs

Typ e	Sequences
RN A	GUCUCUGUGUGCGCCAGAGACACUGGGGCAGAUUAUGGGCCAGCACAGAAUG AGGCCC
DN A	<u>G</u> <u>T</u> <u>C</u> <u>T</u> <u>C</u> <u>T</u> <u>G</u> <u>T</u> <u>G</u> <u>T</u> <u>G</u> <u>C</u> <u>G</u> <u>C</u> <u>C</u> <u>A</u> <u>G</u> <u>A</u> <u>G</u> <u>A</u> <u>A</u> <u>C</u> <u>A</u> <u>C</u> <u>T</u> <u>G</u> <u>G</u> <u>G</u> <u>G</u> <u>C</u> <u>A</u> <u>G</u> <u>A</u> <u>T</u> <u>A</u> <u>T</u> <u>G</u> <u>G</u> <u>G</u> <u>C</u> <u>C</u> <u>A</u> <u>G</u> <u>C</u> <u>A</u> <u>C</u> <u>A</u> <u>G</u> <u>A</u> <u>A</u> <u>T</u> <u>G</u> <u>A</u> GGCCC

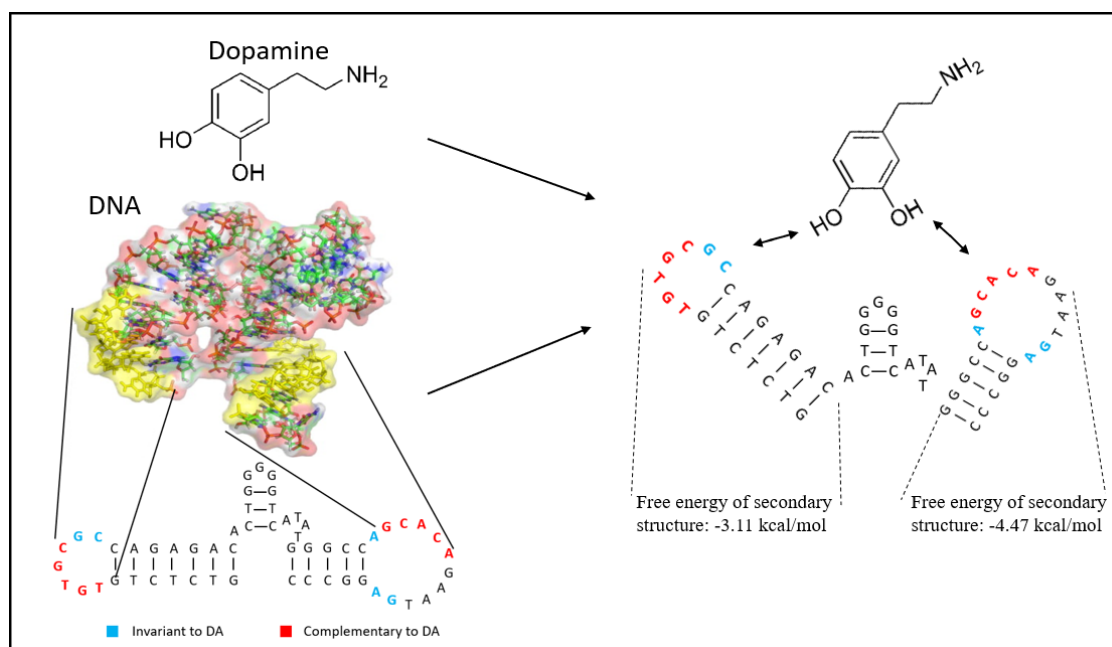


FIGURE 5: Dopamine chemical structure and DNA sequence with complementary (red) and invariant (blue) nucleotides for DNA binding to DA and stem loop exergonic stability.

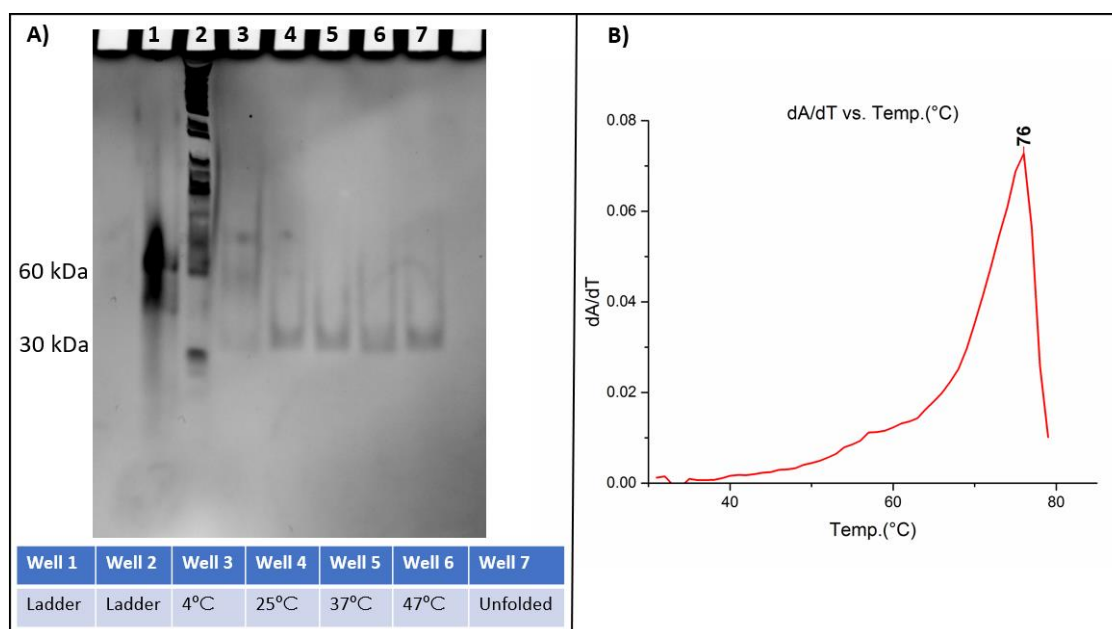


FIGURE 6: DNA aptamer (A) gel electrophoresis test for DNA folding stability at different temperatures, and (B) UV-melting temperature plot for DNA.

#### 2.4 DNA Coupling to GNP Thiol Groups:

Covalent modification is an important strategy for introducing a DNA that will be strongly coupled together with the GNP, which requires covalent bonding of an intermediate group because the DNA negative charge on its backbone only produces electrostatic non-covalent bonding. Thiol, which is a sulfur analogue of alcohol compound with an alkyl (or other organic substituent) attached to sulfhydryl group to form R-S-H, can be modified onto the oligonucleotide DNA strand at its 5' region. Thiol is known to possess strong covalent bonding with GNP surfaces [Orientation and characterization of immobilized antibodies for improved immunoassays (Review)]. By adding three additional thymine nucleotides between the thiol and 5' DNA strand, enough space is created between the DNA and GNP surface that allows the DNA tertiary structure to form without GNP surface constraint interference, but still remain close enough for output signal interaction.

#### 2.5 GNP Plasmonics and Size:

Metal particles possess unique material properties, one such property is their energy conductive surface. It allows high laser absorption much higher than other materials, where they can induce electron excitement for plasma phenomenon. Gold metal particles possess wavelengths near 520-580 nm range that can induce peak plasmon resonance. Changes in GNP diameter can result in slight shifts of wavelengths values corresponding toward peak plasmon values, along with max intensity of electromagnetic field (E-Field) intensity. GNPs between the size of 20-100nm produce the highest E-Field intensity. GNPs at 60nm diameter produce the strongest response at induced wavelength of 550nm, Figure 7, where an input laser intensity of 1V/m electric field will increase to 5V/m. The Plasmon response begins at 470nm, reaches plasmon resonance mode at 550nm, drops sharply at 600nm, then

slowly diminishes at onward past 700nm, Figure 8. As the plasmonic phenomenon enhances, maximum intensity on the GNP occurs near 3-10nm from surface with a near 37.5% difference in maximum intensity between the two spots, Figure 9. This illustrates molecular compounds immobilized on the surface will exhibit the strongest plasmonic intensity's while their bonding regions at the GNP surface will exhibit a slight 30% drop in intensity.

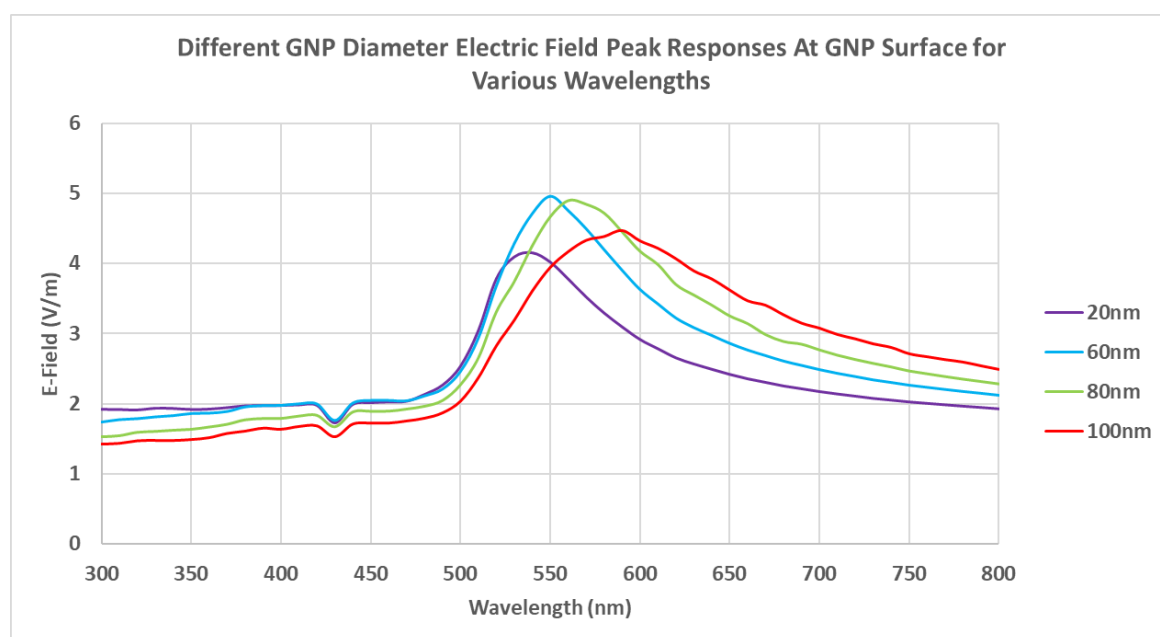


FIGURE 7: Gold nanoparticle plasmonic resonances at Various Diameters

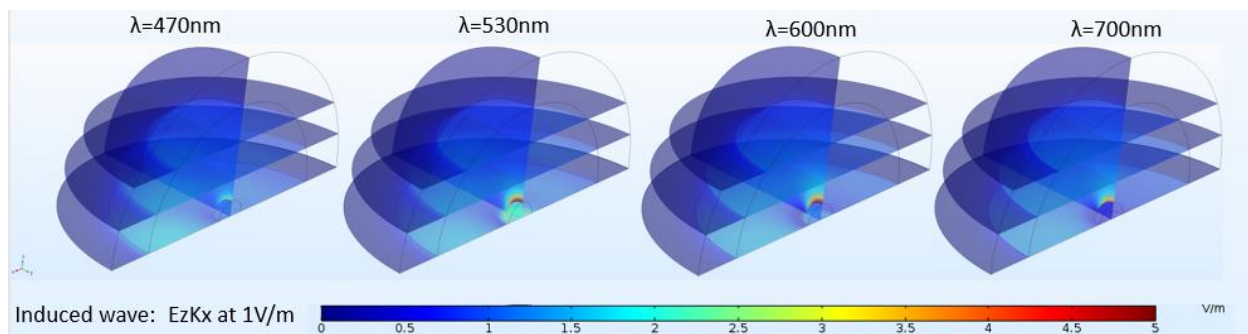


FIGURE 8: 60nm Diameter GNP with induced electric field 1V/m in the EzKx direction, and the plasmonic response at various wavelengths

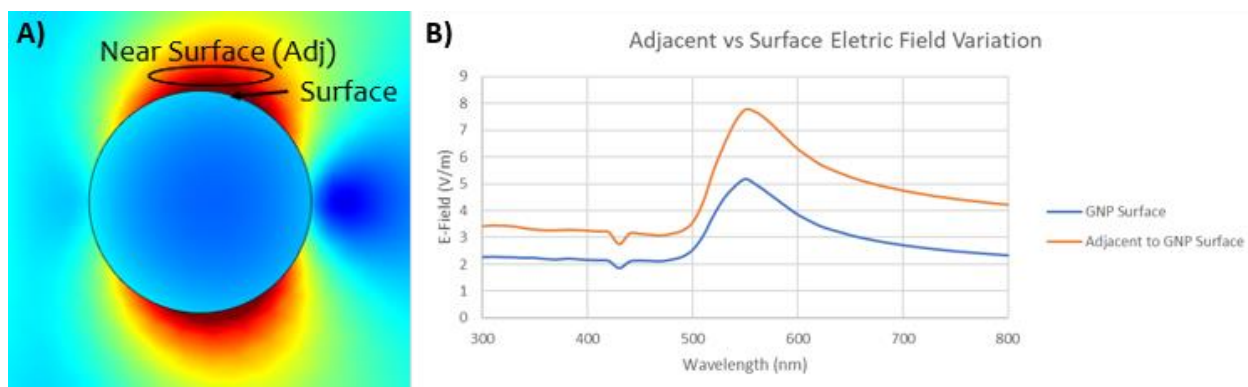


FIGURE 9: 60nm Diameter GNP induced with a 1V/m Electric field for the response (A) at its surface and adjacent toward its surface, and (B) the peak electric field (V/m) pattern for various wavelengths of the two locations.

## 2.6 Fabrication and Essay Design:

Fabrication of both the GNP particle and Probe Chip are a multistep process. The chip is fabricated first, followed the nanoprobe, illustrated in Figure 10. The chip fabrication begins with piranha cleaning the glass slides. The glass slides are then plasma treated for 2 minutes on the same side that was piranha cleaned. Piranha cleaning removes the glass slide of any impurities while plasma treatment excites the surface improved oxidized reaction with chemical coating. The freshly plasma treated glass slide is then submerged in an APS 95% ethanol solution at 3% APS volume ratio for 15 minutes. The

slides are then air dried with N<sub>2</sub> to remove excess solution and homogeneously distribute surface layer, thus completing Stage 1. PDMS, solidified beforehand at a 10:1 ratio of polymer and curing agent, is cut into a 25x15mm rectangle with 2mm thickness. 3mm diameter holes are punched in a 2xN matrix, where N represents number of assay conditions. The PDMS is then plasma treated to energize the Si surface and remove hydrogen. Once completed, the PDMS is then bonding to the glass slide for 30 minutes where the Si-O joins for a strong bond. This completes Stage 2. Stage 3 begins by vortexing a GNP solution, then inserting 20 $\mu$ L into each well for 1hr incubation at 4°C. The cold temperature stabilizes the GNPs while the time 1hr incubation allows adequate time for GNP bonding to the NH<sub>3</sub><sup>+</sup> group for immobilization. Each well with GNP solution is then washed with deionized water at 20 $\mu$ L for three cycles to insure all unbound GNPs are removed. This completes Stage 3. Next, a DNA sample was formed with a DNA buffer at 7.5 pH containing NaCl<sub>2</sub>, Tris, and MgCl for a DNA solution. The solution was then incubated in DTT for removal of a thiol cap for 20 minutes, then filtered through a gel extrusion to separate the DNA from the now removed thiol cap and DTT by electric charge and size constraints of the gel. DNA is then heated in at 90°C for 2min to loosen the oligonucleotide and separate any undesired base-pair bonding during DTT and gel extrusion, then submerged in an ice bath for 2min to stabilize proper tertiary structure. The DNA solution was then injected at 20 $\mu$ L into wells, then stored in 4°C for 1hr, giving DNA adequate time to for the thiol group to bond with the GNP surface. After 1hr, each well is washed three times with 20 $\mu$ L of DNA buffer to ensure all unbound DNA strands are removed, thus completing platform and probe fabrication.

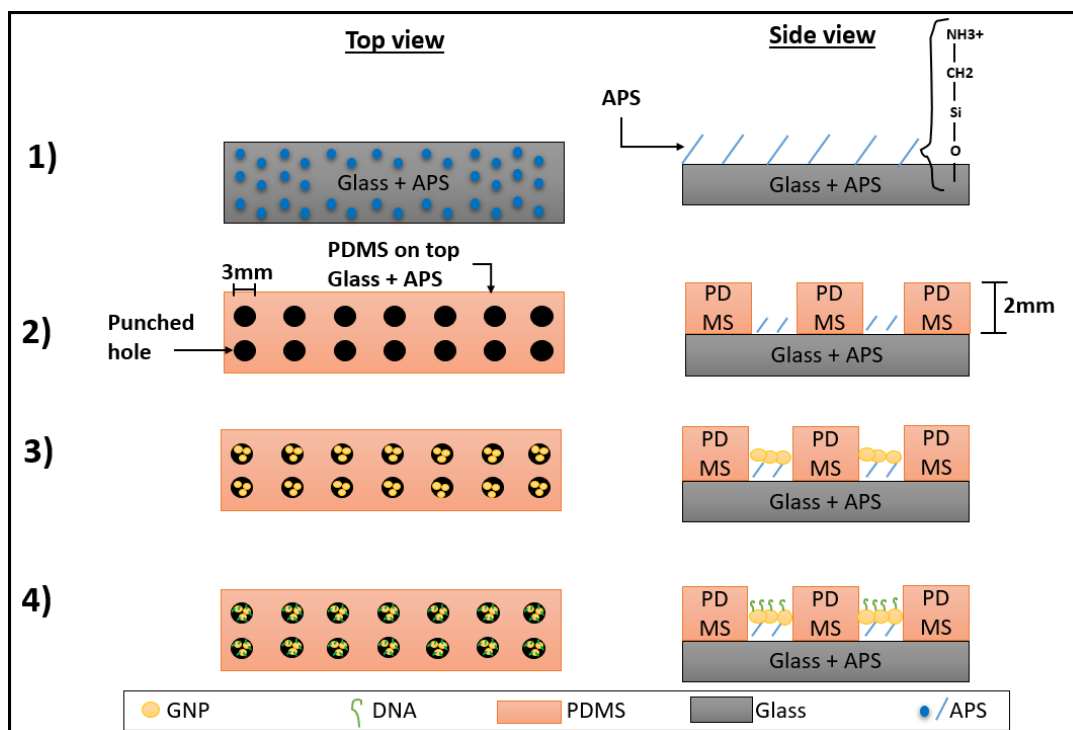


FIGURE 10: Platform and DA-probe fabrication from (1) APS coating onto glass, (2) PDMS bonding to glass slide, (3) GNP insertion and (4) DNA insertion.

Dopamine is then added into the system at various concentrations depending on assay conditions. Similar to DNA and GNP incubation, the DA is incubated for 1hr at 4°C, followed by three times washing with DNA buffer to remove any unbound DA. Care flowrates at low velocities are used during washing to avoid any accidental induced separation of DA bound to DNA. After DA preparation, SERS measurement is applied. The SERS microscope begins by applying laser signal through a separation lens, that is then joined by a Band Pass APD input, followed by laser guidance and adjusted toward the surface where it hits the target GNP cluster by specially designed lenses. The induced laser at 530nm and 30mW power is absorbed by the probe cluster, excited by the plasmonic effect, then emitted back through the objected lens at 50x. The laser scans the surface with an excitation time of 5 minutes. The returning signal will possess an emission with Glass,

GNP, DNA, and DA Raman spectra's that are separated by Raman filters, then guided toward a spectrometer for signal assessment. Here, the change in wavelength pattern develops the SERS graph. Figure 11 details the DA SERS experiment.

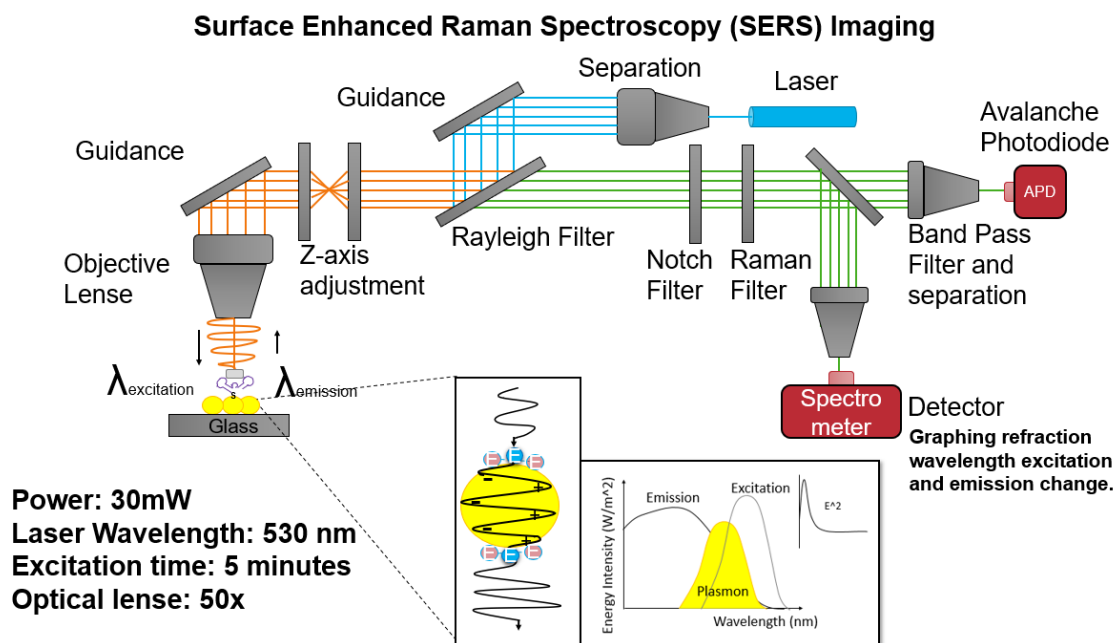


FIGURE 11: SERS application of a DA-probe measurement.

## 2.7 Platform and Probe Verification:

All conditions for the probe design and platform fabrication were validation for operation. Each condition includes the APS coating, PDMS bonding with glass, GNP immobilization onto the glass surface, bioreceptor stability, bioreceptor bonding to DA, and DNA bonding with GNP. APS must coat the glass surface with enough concentration that guarantees high coating. Hydrophobic and hydrophilic properties of material was used to validate the APS coating, as glass surface with cleaner surfaces exhibits more hydrophilic characteristics while glass with APS coating will exhibit hydrophobic characteristics. When a water droplet is applied to the surface, the drop will spread out in

hydrophilic contact since there is fewer force resistance, this produces a flatter droplet with a lower angle to the surface. Droplets applied on a hydrophilic surface will maintain more of a spherical shape as the surface repels the droplet boundary from spreading, this forms a higher droplet angle with the surface. Figure 12A below demonstrates piranha cleaning increases the hydrophobic property of glass surface with its coating, the plasma treatment purifies the surface creating a strong hydrophilic surface of glass, then APS coating creates a strong hydrophobic surface due to its chemical coating. The droplet angle of water after APS coating shows an angle shift from 10 to 40 degrees, indicate strong APS coating. Angles measurement is shown in Figure 12B.

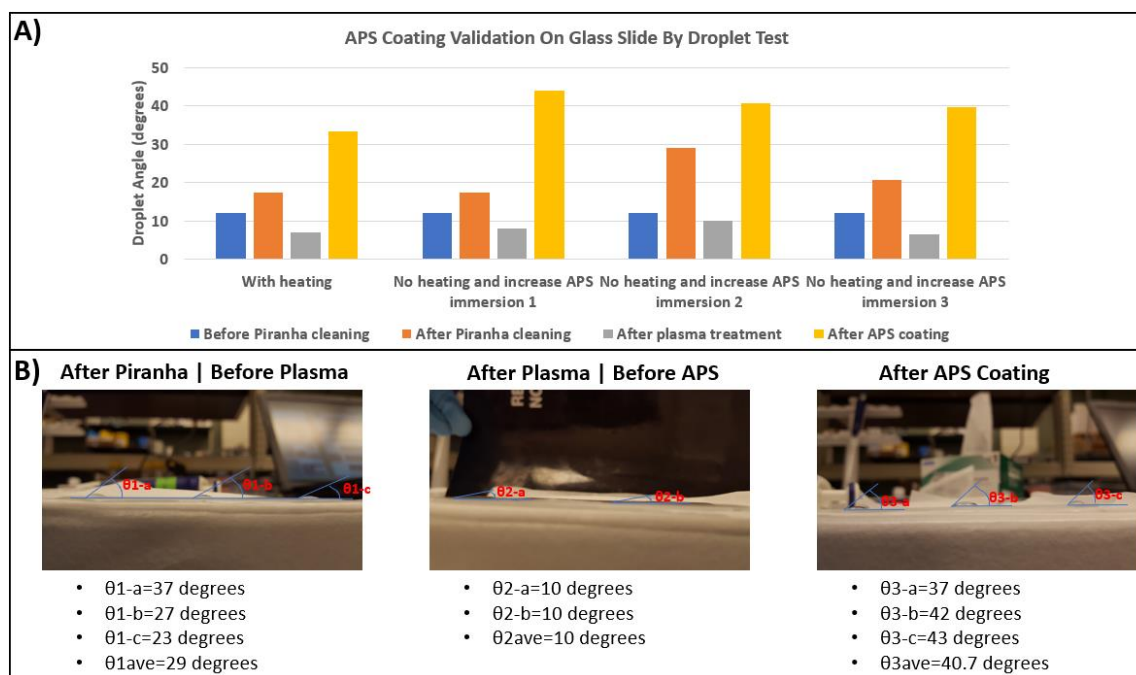


FIGURE 12: APS coating validation by water droplet test. (A) Statistical assessment between hydrophobic or hydrophobicity of glass cleaned and with or without APS, and (B) droplet angle assessment.

The immobilization of GNP to the APS coating was validated by a Darkfield microscope at 20x, 50x and 100x lense. Darkfield is a microscopy method that filters the

unscattered reflected beam from the GNP coated surface. This results in areas surround GNP (i.e., no GNP) reflecting a generally dark region. The essay condition involved four Darkfield images taken at no washing, one washing, two washings, and three washings to observe if any quantification of GNPs that were removed and how much remained immobilized by the APS for first iteration, Figure 13A, and immobilization degree from continuous washing, Figure 13B. In the initial stage, GNPs show a homogeneous coating at high concentration as tiny green dots (aggregations demonstrate a color shift to red for GNPs). Upon first washing, about 15% was removed, leaving a small 100-300 $\mu$ m GNP clusters randomized throughout the surface. The second and third washing events detail only about 1-5% of GNP concentration was removed, detailing immobilization was achieved for GNPs with about approximately greater 80% GNP remaining. Aggregation of GNP was observed by incubating GNP with CuSO<sub>4</sub>. CuSO<sub>4</sub> has a strong negative charge that groups the GNPs together by their positive charges. Figure 14 shows the GNP aggregation after three times washing, here the GNPs remain immobilized. 1mM of CuSO<sub>4</sub> shows high aggregation by their GNP red color, while 5mM CuSO<sub>4</sub> shows excessive ratio as CuSO<sub>4</sub> aggregates onto of the GNP aggregation, shown by its partially white color.

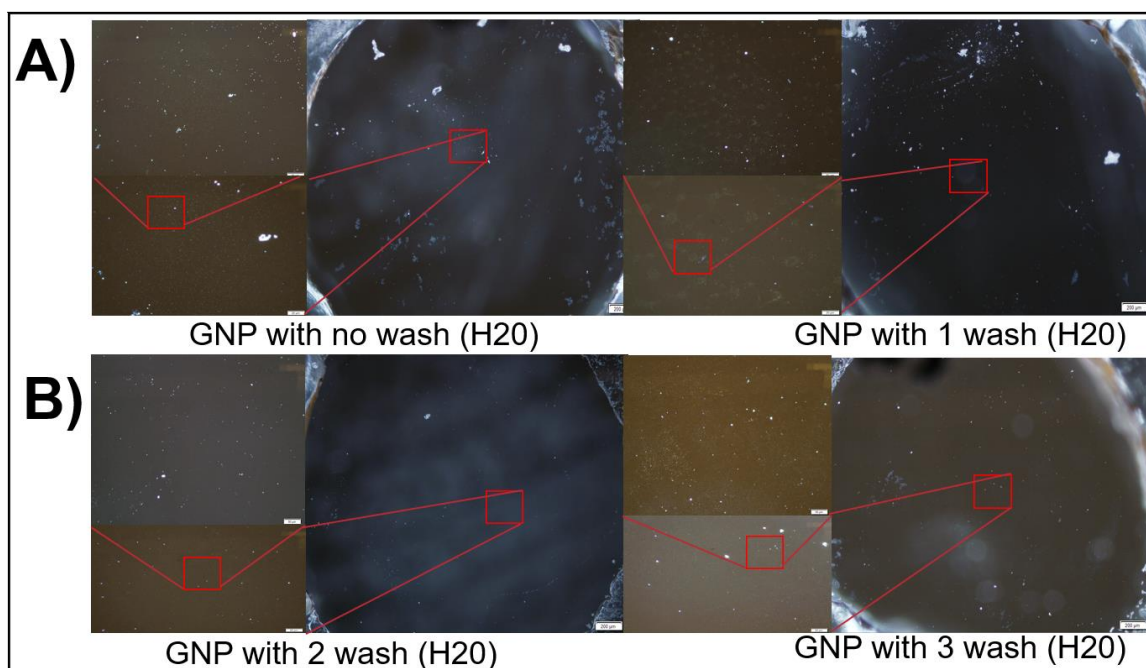


FIGURE 13: GNP immobilization observed at (A) zero, left, and one wash, right, and (B) two times wash, left, and 3 times wash, right (scale bar 200µm).

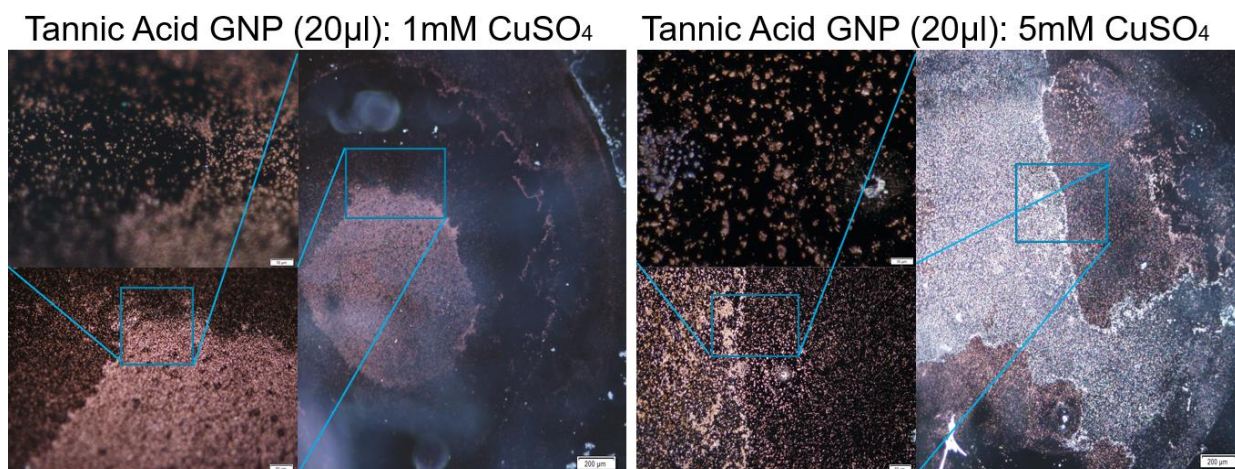


FIGURE 14: GNP aggregation induced by CuSO<sub>4</sub> (scale bar 200µm).

PDMS bonding strength to glass can be hindered by the intermediate APS coating, as such, a weak bondage will result in GNP solution leaking in-between the PDMS and glass/APS coating. Plasma treatment power level is the main factor of inducing bonding

strength between PDMS and glass by the power level's capability to energize the Si on the PDMS and O on the glass. Higher power levels improve energy induction, however, as the power increases, so does the induced damage on the APS that can cause the coating to be removed. As such, there exists an intermediate optimized power level for plasma treatment that can prevent GNP leakage while insuring GNP immobilization. An assay was conducted at three different power levels to evaluate the optimized condition with 25 cc/min air flow associated with a low plasma power, a medium plasma power, and a high plasma power. After the plasma treatments, PDMS was bonded to the glass then GNP solutions were added to the wells for 1hr incubation. Dark Field was used to image in the center of the wells and underneath the PDMS and well edge. If plasma treatment was too weak, leakage will exist by showing GNPs underneath the PDMS, and strong layer of APS will remain showing high concentration of GNPs in the center of the well that are immobilized, if plasma treatment was too strong, no leakage exist showing no GNPs under the PDMS, but there will also be high APS damage resulting in little to none GNP coating in the center of the well. An optimized plasma level will show GNPs remain while little to none exist under the PDMS, Figure 15A. The low plasma treatment exhibit leakage, along with high concentration of GNP immobilization, Figure 15B left column, high plasma treatment showed weak GNP immobilization at 100x lense, and no leakage, Figure 15B right column, and medium plasma showed a maintained GNP immobilization, Figure 15B middle column. This validates plasma power optimization for PDMS bonding.

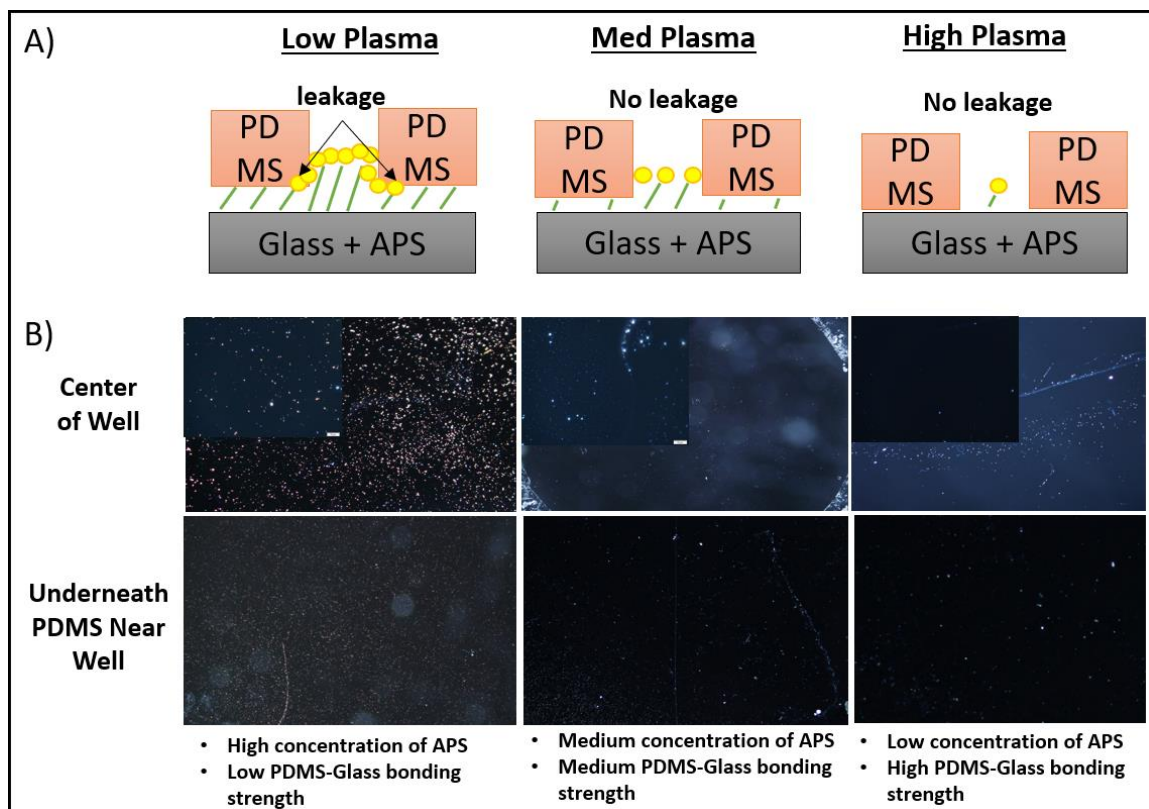


FIGURE 15: Plasma treatment level optimization (A) at three different power levels and (B) their corresponding effect on GNP coating with APS and GNP leakage through PDMS (scale bar 200 $\mu$ m).

The ability for the DNA to bond to the GNP, showing the thiol cap was properly removed and the thiol element engages in covalent bonding, was demonstrated by utilizing the same DNA strand with a TEMRA fluorescence dye attached to the 3' end, DNA-FL. Here, the experiment was conducted on a 96 well plate with a fluorescence reader. The fabrication was conducted the same with APS coating onto glass, GNP coating for 1hr with three times washing, and DNA-FL coating for 1hr with three times washing. The design would show a signal increase by comparing wells with DNA-FL compared to wells without DNA-FL. The TEMRA dye possesses an 530/590 excitation emission spectra. Signals for the DNA-FL were measured at concentrations at 1250 nM, 1000nM, 200nM, 150nM, 100nM, 50nM and 15nM, the limit of detection was shown to have fluorescence signal at

concentrations as low as 15nM and a 75% linear range between 15nM-200nM, illustrated in Figure 16 A. The DNA-FL coupling to GNP was validated at two different essays, one demonstrating concentration differences of DNA, Figure 16B, and another detailing application with and without DTT, Figure 16C. Both conditions have negative controls of just GNP without DNA. A washing condition shows GNP remains in all samples (a larger portion was washed away as 96 well plate surface possesses less surface area coverage for GNP bonding). The concentration differences, 800nM and 400nM, were assessed at all three washing stages. Fluoresce signals are measured by FL intensity on the left axis, and GNP absorption was measured on the right axis (detailing the remaining concentration of GNP). The negative control for just DNA-FL and GNP-DNA-FL at 800nM showed a near 50% drop in signal intensity upon first wash, this indicates there was significantly more DNA than GNP bonding surface area coverage available (as indicated by the drop in GNP washing). The second wash showed a 6% drop and the third wash showed a 4% drop in signal, with all signal intensities remaining significantly higher than the negative control for just GNP signal. The GNP absorption shows less than 10% of GNP was lost during washing. At 200nM DNA-FL, the non-washing negative controls DNA-FL with and without GNP, showed a near 28% drop in signal intensity after first washing (showing again removal of unbound DNA-FL as there exist more DNA-FL available than GNP surface area coverage), then less than 2.5% drop in the second and third washing. All signals for the 400nM remained above the negative control without DNA-FL threshold. These tests demonstrate DNA at various concentrations does bind to GNP, although higher concentrations will be lost if there doesn't exist the appropriate GNP surface area coverage. Further assessment validates these results were not exhibited by false positive imaging

from electrostatic bonding of DNA to well edges, and that the removal of thiol cap with DTT incubation was necessary. This was conducted by implementing a condition for just DNA-FL without GNP for electrostatic assessment, and a condition for DNA-FL without DTT incubation for DTT quality assessment, where each one possessed a well without washing showing natural signal, then subjected to washing where their respective signals should significantly drop. Compared to DNA-FL with DTT removal and immobilized GNP for bonding, all three conditions showed relative similar intensities prior to washing, then after the first washing cycle, both negative controls showed a near 40% drop while the positive control showed less than a 4% drop. Second washing condition demonstrated about 8% drop for all three conditions. All three conditions showed signals above negative for no DNA-FL, indicating DNA-FL remained in all three. This indicates some of the DNA-FL's electrostatic force can bond to the edge of the well surface, and to GNP surface. However, removal of the DTT is required for optimized DNA coating.

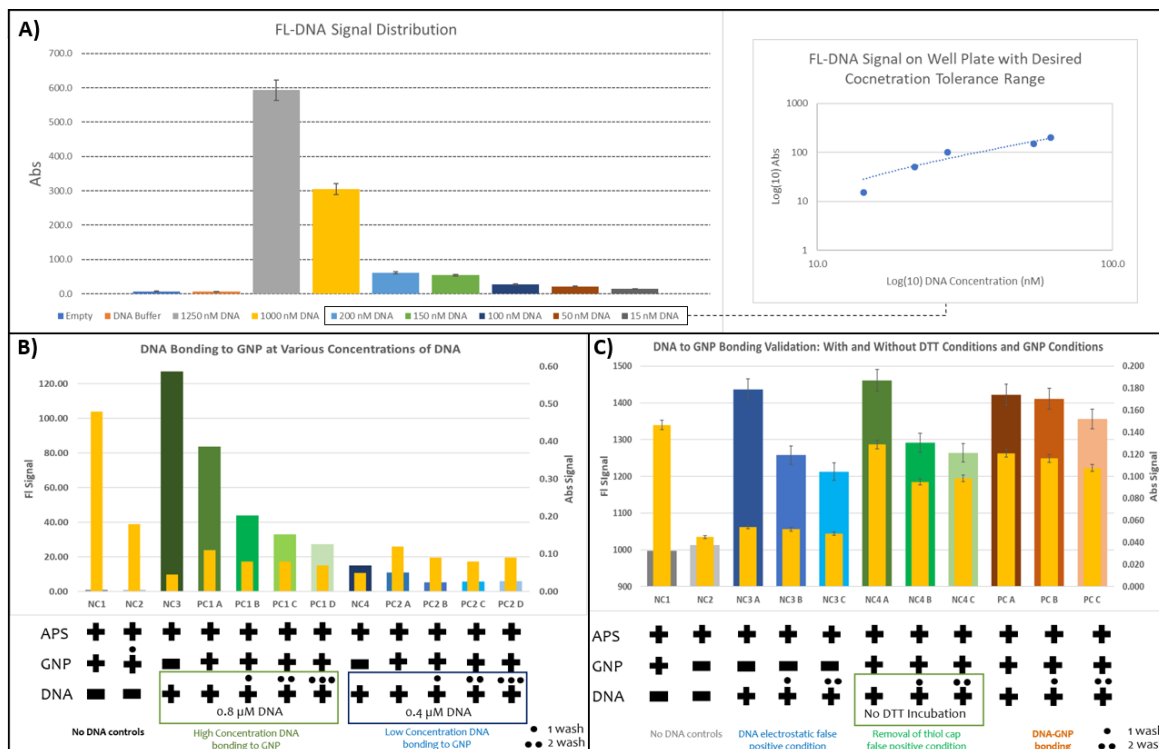


FIGURE 16: TEMRA dye attached to DNA fluorescence signals. (B) DNA-FL concentration differences and corresponding GNP binding capabilities, and (C) DNA-FL DTT removal validation.

The DNA capability to bind to DA was validated by a gel electrophoresis test utilizing a Fluoresce stained dopamine (DA-FL) with excitation 333nm and emission 515nm. Experimental design was constructed with a negative control condition containing only DNA at a concentration of 5 $\mu$ M stained with ethidium bromide (EtBr) producing a red signal, a negative control condition with just DA-FL measured at a green signal with a low concentration of 50 $\mu$ M and high concentration of 100 $\mu$ M. The DNA has a band at 30kDa while the DA-FL has a band at 60kDa. Positive control conditions containing both DNA and DA-FL demonstrated the DNA bonding with DA-FL and by pulling it downward into the 30kDa range, where otherwise DA would not be able to reach the 30kDa band section on its own. The gel was comprised of 10.5 H<sub>2</sub>O, 3mL 40% acrylamide/bis-

acrylamide, 1.5mL 10x TB, 30 mL 1M MgCl<sub>2</sub>, 9mL TEMED, 150 microliters APS 10%. Figure 17 details 10 separate channels, first one for ladder kDa reference, second and third for DNA signal negative control (high concentration was used to insure high probability for DA bonding that can pull down signal identification), fourth containing no chemicals for back ground negative control, fifth and sixth for DA-FL at 50nM and 100nM, respectively, 7<sup>th</sup> and 8<sup>th</sup> for DNA and DA-FL at 50nM where one was incubated together for 1hr prior to gel and the other was incubated upon gel channel insertion, and 9<sup>th</sup> and 10<sup>th</sup> channel repeating same conditions, but instead with 100nM DA-FL. Channels with DNA and DA-FL demonstrated DNA did bond with DA-FL by a green signal at 30kDa. Only 5nM of DA-FL were pulled down as there was only 5nM of DNA. Incubation showed slightly higher bonding rate with DA-FL.

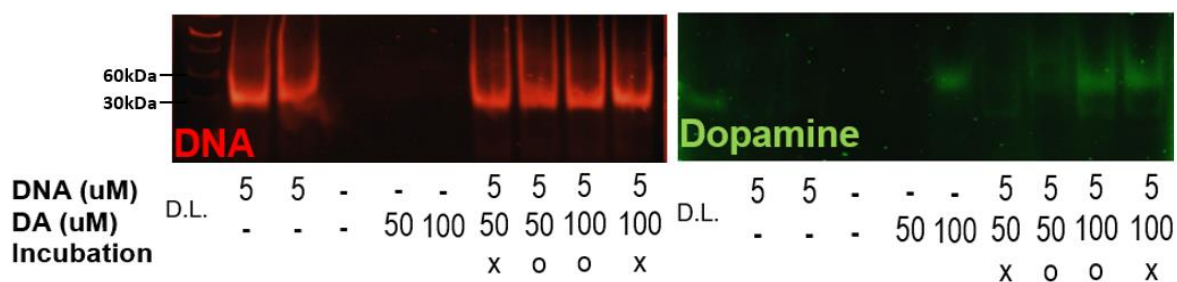


FIGURE 17: DNA bonding with DA-FL by a gel electrophoresis essay

## 2.8 Platform Material List:

The material list for the project consist of tannic coated gold nanoparticles from TED Pella, Inc, dopamine, labeled dopamine, tyrosine and norepinephrine molecules from Sigma Aldrich, DNA aptamer and fluoresced labeled DNA aptamer from IDTDNA, PDMS from Slygard, glass slides from Sigma Aldrich, MgCl<sub>2</sub>, NaCl, and Tris from Thermo

Fisher. Equipment includes hooded ventilation, dark field microscopy, fluorescence microscopy, SERS microscopy, centrifuge, and piranha clean chemical hood.

## CHAPTER 3: RESULTS AND DISCUSSIONS

### 3.1 Dopamine Nanoprobe:

Applications for monitoring Parkinson's Disease (PD) require nanosensor technology with biofriendly material integrated with high sensitivity and specificity design features. A PD-sensor must be able to detect DA without false positive signaling from similarly structured molecules while possessing high resolution to relaying small concentrations of dopamine to a format distinguishable to the researcher. Here we present a probe utilizing the design for biological recognition by a DNA aptamer stem loop that will recognize small specific regions of the dopamine protein via a specific nucleotide complementary sequence. The DNA is sequenced with thiol, a sulfur hydroxyl group in alcohol, that covalently bonds to a gold nanoparticle (GNP). The gold is fabricated in the shape of a 60nm diameter tannic acid sphere. The gold operates as a plasmonic enhancer to increase the response signaling of the probe. Assembly of the nanoprobe includes aggregation of GNPS by electrostatic bonding with  $\text{CuSO}_4$ , then coating with thiol-DNA aptamers. The aggregation of GNPs along with the plasmonic effect produce higher resolution capabilities. When a DA molecule is present within proximity of the nanoprobe, the DNA binds the DA to the probe to create a signal change. The signal utilized is a Raman Spectra induced laser to excite the probe with increased energy. By implementing a large volume of nanoprobes with the plasmonic aggregation enhancement within a system, the accumulation of energy by the laser excitation can reach high enough levels for detection at low concentrations. Control of the Raman signaling is incorporated by immobilizing the GNPs by electrostatic bonding with APS coated on top of glass. The tannic acid on the GNP surface increases the GNPs electrostatic to APS strength when aggregated with other

GNPs, this allows a higher surface area coverage for improved results. As the induced wavelength is absorbed by the probe, the plasmonic surface (electrons covering the surface) transfers its energy its own wavelength and the induced wavelength converge. When the probe absorbs the energy, it becomes unstable and emits the energy where the wavelength can be measured. The spectra of the wavelength are dependent of the molecular weight of the whole probe. The molecular weight of the probe can vary from aggregate and singular GNPs, GNPs with DNA, and GNP+DNA+DA at different concentrations of DA. The response varies at different emissions of  $\text{cm}^{-1}$ , these variations detail the library contributing the presence of dopamine, and the degree of dopamine concentration.

### 3.2 Raman Spectra of Components:

The Raman spectra for GNPs shows a first mode plasmon band near  $1200 \text{ cm}^{-1}$ , and a second plasmon mode with broad band between  $1500\text{-}1611 \text{ cm}^{-1}$ , containing a sharp internal band between  $1590\text{-}1611 \text{ cm}^{-1}$ . The plasmonic peak shows high amplification in the intensity, Figure 18A, from large clusters of GNPs, Figure 18B. The large band extruding past the  $1600 \text{ cm}^{-1}$  region illustrates Raman of glass. Raman spectra of DNA resembles glass, showing DNA cannot be measured nor seen on the 100x lense, Figure 18C and Figure 18 D, respectfully. Dopamine shows a first Raman peak near  $700 \text{ cm}^{-1}$ , a second peak near  $1280 \text{ cm}^{-1}$  due to its carbon groups, a third strong peak near  $1611 \text{ cm}^{-1}$  due to its double bonds, and a strong cluster of peaks near its  $3000 \text{ cm}^{-1}$  regions due to its oxygen emission, Figure 18 E. Dopamine was taken from a 5mg powder, Figure 18F.

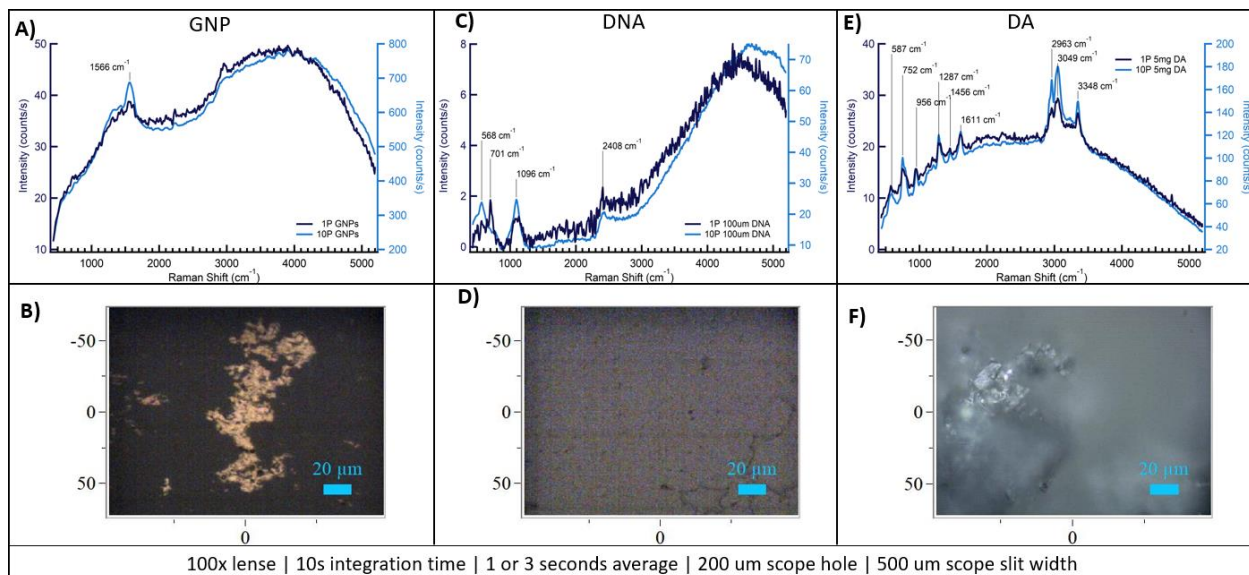


FIGURE 18: Raman spectra's of (A) GNP and its (B) visual fluorescence image, (C) Raman spectra's of DNA and its (D) visual fluorescence image, and (E) Raman spectra's of dopamine and its (F) visual fluorescence image.

### 3.3 Dopamine Nanoprobe Detection:

The input power used by the SERS laser effects a large portion of the probe response. Too low power will result in an unmeasurable readout, too high of a power can induce the plasmonic effect to extreme conditions on the DNA and deteriorate the bioreceptor. Utilizing a SERS microscope with 1% power, 10% power, and 25% power of 300mW, a 100x microscopic lens, 10sec integration time, 1 to 3 second averaging, 200 $\mu$ m scope hole, and 500 $\mu$ m slit width, showed calibration of GNP-DNA matching patterns of GNP Raman spectra, with spike band between 1175-1611 $\text{cm}^{-1}$ , and a large internal spike at 1590 $\text{cm}^{-1}$  to 1630 $\text{cm}^{-1}$ . Glass showed Raman spectra at 590 $\text{cm}^{-1}$  and 1130 $\text{cm}^{-1}$  with a large rise after 2400 $\text{cm}^{-1}$ . DA showed similar DA fingerprint with spikes at 757 $\text{cm}^{-1}$ , 1291 $\text{cm}^{-1}$ , 1452 $\text{cm}^{-1}$ , 1611 $\text{cm}^{-1}$ , 1267 $\text{cm}^{-1}$ , 3064 $\text{cm}^{-1}$ , and 3357 $\text{cm}^{-1}$ . Figure 19 illustrates the calibration.

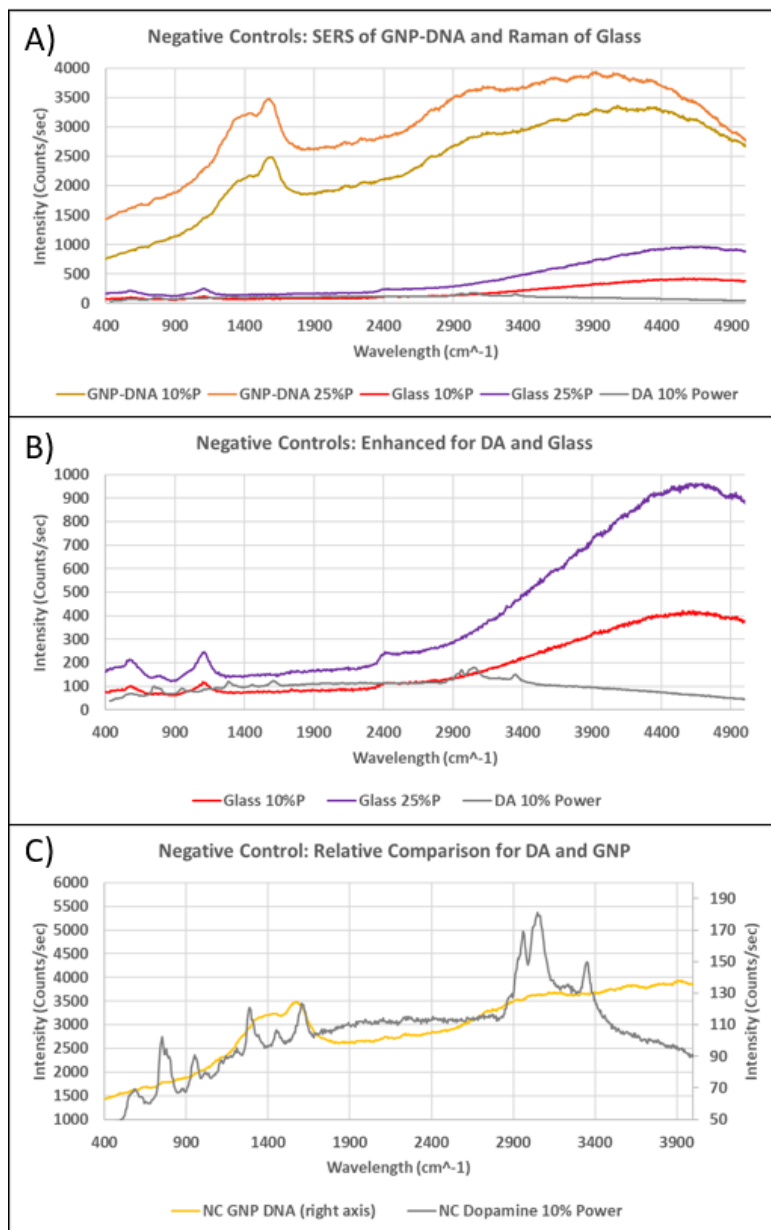


FIGURE 19: (A) SERS Calibration with probe components, (B) enhanced for glass and DA Raman spectra, and (C) comparison between DA and GNP spectra.

Once calibrated, the SERS was initiated at different power levels and aimed at different DA-probe aggregation levels to induce different plasmonic responses. DA at concentration of 1mM was used to set standard reference point for DA sensitivity. The SERS measurements demonstrated at 10% power the left band from 1170cm<sup>-1</sup> to

1520 $\text{cm}^{-1}$  increased in intensity, matching the intensity of the internal GNP peak. Additionally, the internal peak expanded to 1590 $\text{cm}^{-1}$  to 1630 $\text{cm}^{-1}$ . 25% Power showed damage and dissemble from too extreme power levels with a diminish in GNP response, Figure 20A. Compared to NC GNP-DNA, presence of DA shows expansion of main GNP band with increase in left band that matches right band, Figure 20B. Compared with DA spectra, Figure 20C, this phenomenon is responding toward the three DA spikes near 1400 $\text{cm}^{-1}$ . However, none of the sharp DA spike characteristics are present. Increased DA-nanoprobe aggregation, similar pattern with the presence of DA showing an increase in the leftward 1500 $\text{cm}^{-1}$  region, Figure 21A. Compared to GNP-DNA reference, this pattern shows similar distinction, Figure 21B. Compared to DA reference, the spikes near 1400 $\text{cm}^{-1}$  appear to be influencing the near 1500 $\text{cm}^{-1}$  band, however, no DA fingerprint spike response were observed, Figure 21C. The surface appearance of GNP-DNA bonded with DA shows a distant dark surface overlapping a yellow/red surface. Once SERS is applied to the surface, the dark distinction of DNA-DA disappears leaving a bright plasmonic surface activated from the GNP, Figure 22A. This indicates 10% power is enough to enact over powered SERS plasmonics. Imagining SERS on the same location shows a strong drop in intensity with a loss of the 1500 $\text{cm}^{-1}$  DA pattern, Figure 22B.

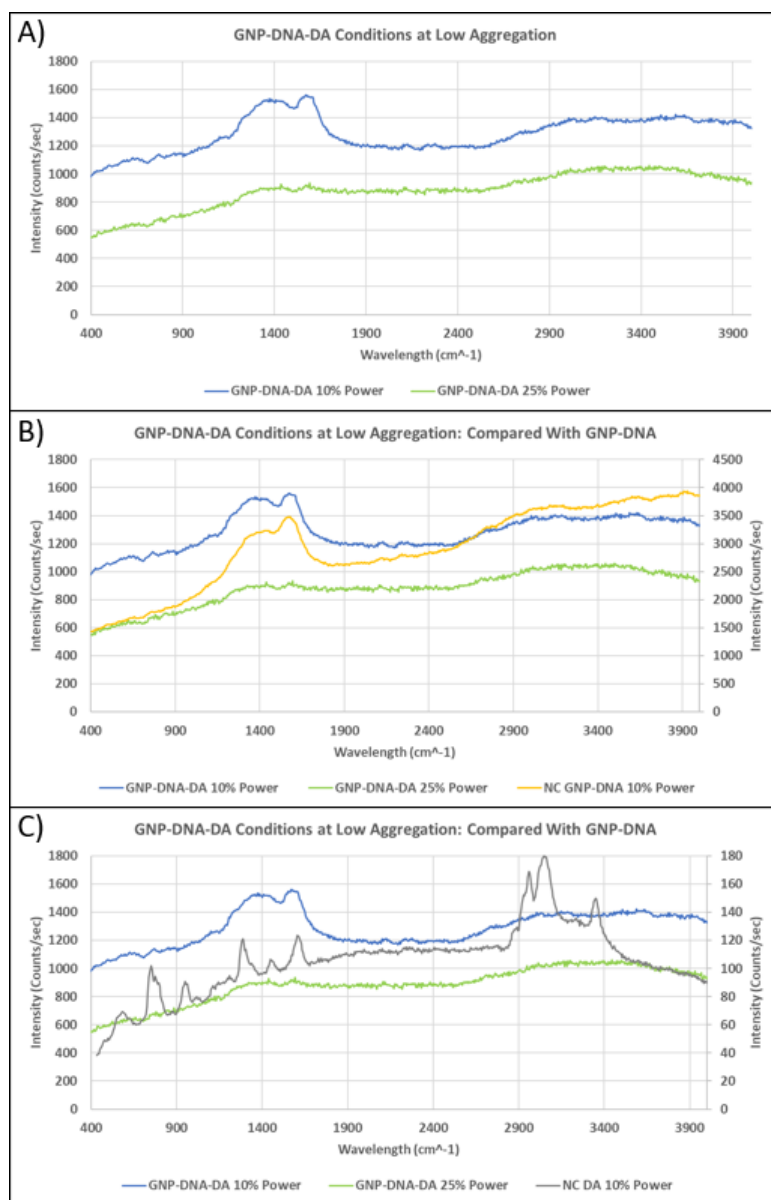


FIGURE 20: Detection of 1mM DA with GNP-DNA-DA probe at (A) low aggregation, (B) compared with GNP-DNA reference, and (C) compared with DA reference.

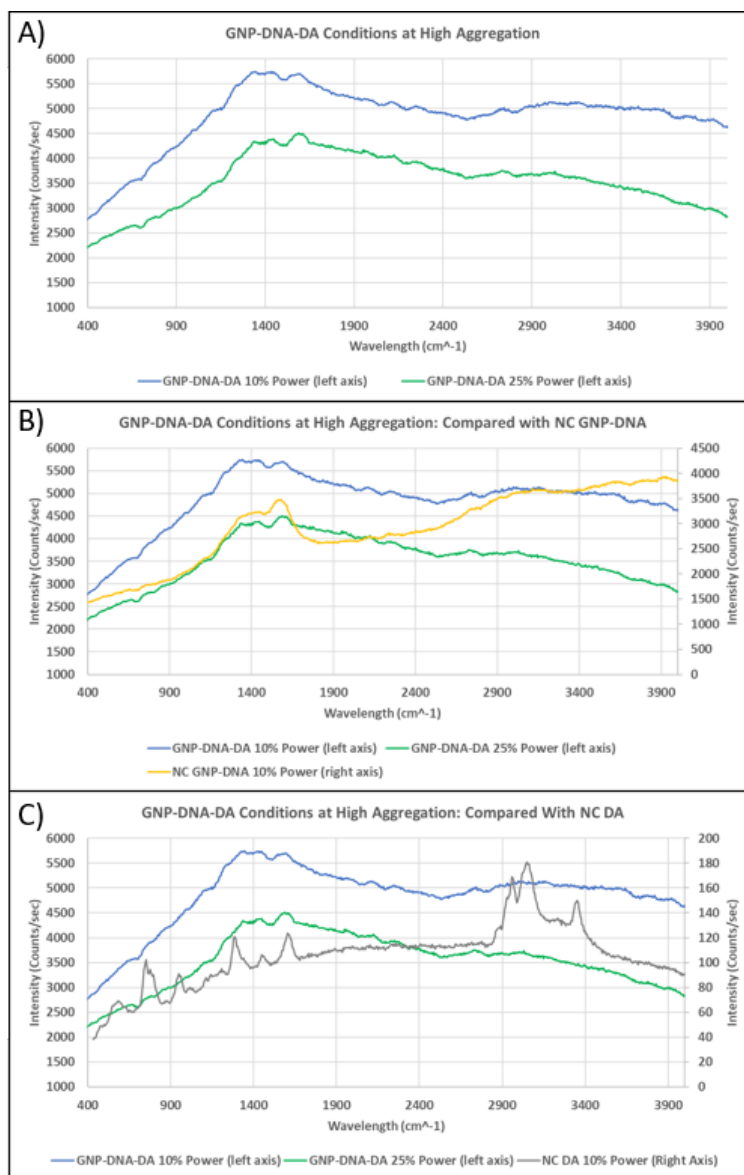


FIGURE 21: Detection of 1mM DA with GNP-DNA-DA probe at (A) high aggregation, (B) compared with GNP-DNA reference, and (C) compared with DA reference.

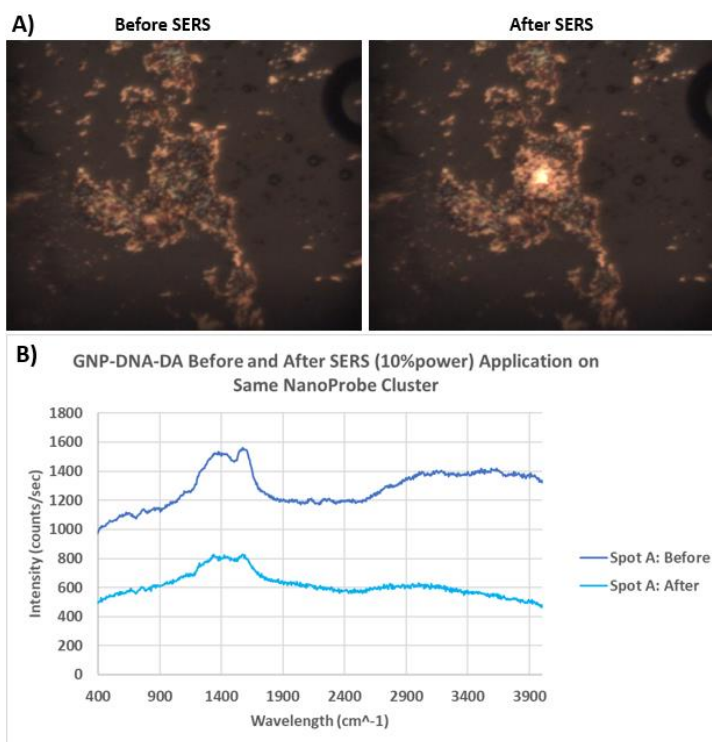


FIGURE 22: (A) GNP-DNA-DA cluster before and after activation of SERS (10% power). (B) SERS response from first iteration of SERS and second iteration of SERS.

The shift in the 1500cm<sup>-1</sup> GNP band in presence of DA and its 1400cm<sup>-1</sup> three spike regions, but lack of sharp DA spikes from other fingerprint regions, indicates DA is bonding with the bioreceptor, until the first cycle of SERS application removes the Bonding. The SERS operates in three cycle per measured surface area, where the first cycle picks up and removes the DA signal measuring a partial DA signal, then the other two signals average and dilute the response with non-DA (heated plasmonic removing the DA) measurements. This indicates a new SERS power level is required below 10% of 300mW. A new SERS laser was selected with higher power percentage resolution while still utilizing same parameters as before. Calibration of probe components at 5% power of 300mW shows sharper DA band peaks and GNP peaks, Figure 23. Further experiments are projected to be performed here to acquire sensitivity LOD and LR and selectivity against

tyrosine and NE upon DA calibration. Expected results based on plasmonic enhancement and new sharp DA peaks are around the range of 0.8pM to 50nM resolution.

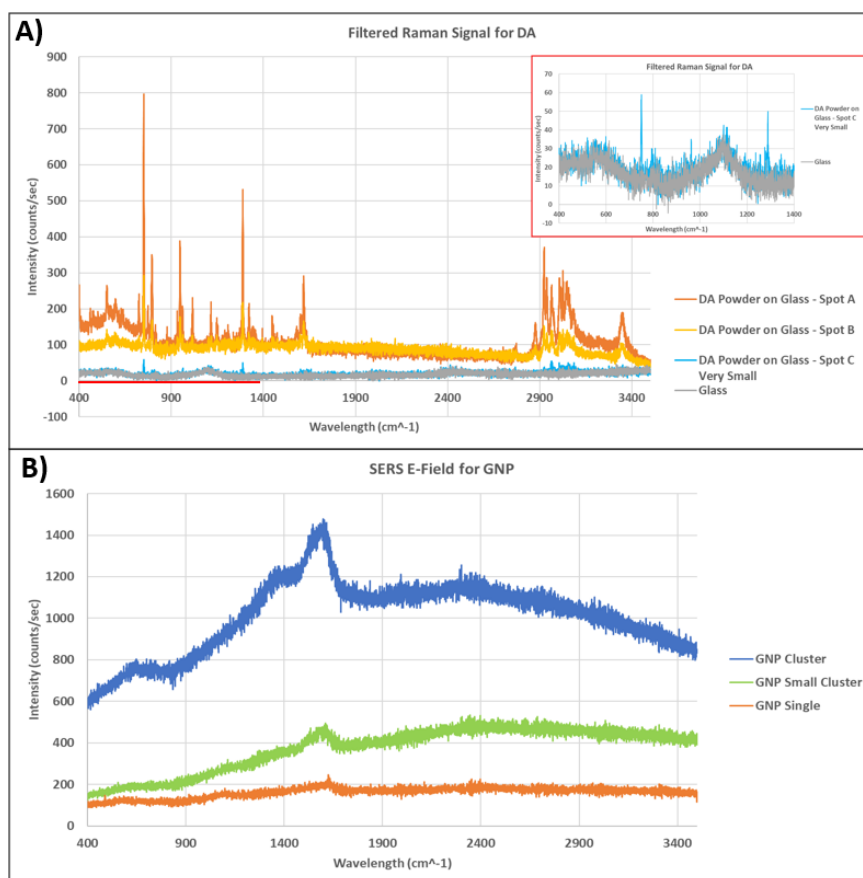


FIGURE 23: SERS calibration of (A) DA and (B) GNP

## CONCLUSION

Here, a dopamine (DA) nanoprobe was designed for Parkinson's Disease (PD) stage signaling with SERS by measuring the associated response of DA reduction at low concentrations. The nanoprobe utilizes a DNA aptamer as a bioreceptor and a gold nanoparticle (GNP) for signal enhancement. Fabrication validation indicated the probe achieves stability for DNA coupling to GNP and DNA bonding to DA while producing a SERS plasmonic enhancement  $10^{10}$  fold. The test was conducted within a platform fabricated multi-well PDMS polymer bonded to glass. The platform was validated with PDMS-glass induced stress for bonding strength, hydrophobicity droplet test for APS coating, and dark Field Microscopy for leakage and GNP immobilization. The biological component, DNA aptamer, was validated for its temperature induced thermodynamic stability and dopamine bonding by NATIVE Gel electrophoresis. The probe itself was tested with 30MW Raman Spectra equipment. APS+GPS showed around a 50% increase in signal with narrower spikes from the reference point APS. Results indicate nanoprobe sensitivity is expected to relay a linear range of 1nM-1 $\mu$ M with a limit of detection at 0.75nM while selectivity of probe is expected to relay stronger bonding toward DA against similar structured molecules. Future plans include in vitro neuron chip coated with PD neurons and DA-probe to measure DA levels for neuron-neuron communication.

## REFERENCES

1. Cutler, Eric G. *Project Performance Specification Template R3 UNCC\_NANO*. Rep. Mechanical Engineering and Engineering Science, UNCC-The William States Lee College of Engineering.
2. Cutler, Eric G. *UNCC\_NANO\_ProjectPlan\_Original*. Rep. Mechanical Engineering and Engineering Science, UNCC-The William States Lee College of Engineering.
3. "Retention of Function in the DNA Homolog of the RNA Dopamine Aptamer." *Biochemical and Biophysical Research* (2009)
4. " *The Neurobiology of Parkinson's Disease*. N.p., n.d. Web. 25 July 2016.
5. Agarwal, Atul. "Chapter-25 Dopamine Agonists in Parkinson's Disease." *Parkinson's Disease and Movement Disorders* (2005): 197-200. Web
6. Cho, Hansang, Erh-Chia Yeh, Raghu Sinha, Ted A. Laurence, Jane P. Bearinger, and Luke P. Lee. "Single-Step Nanoplasmonic VEGF 165 Aptasensor for Early Cancer Diagnosis." *ACS Nano* 6.9 (2012): 7607-614. Web.
7. Walsh, Ryan, and Maria C. Derosa. "Retention of Function in the DNA Homolog of the RNA Dopamine Aptamer." *Biochemical and Biophysical Research Communications* 388, no. 4 (2009): 732-35. doi:10.1016/j.bbrc.2009.08.084.
8. Farjami, Elaheh, Rui Campos, Jesper S. Nielsen, Kurt V. Gothelf, Jørgen Kjems, and Elena E. Ferapontova. "RNA Aptamer-Based Electrochemical Biosensor for Selective and Label-Free Analysis of Dopamine." *Analytical Chemistry Anal. Chem.* 85, no. 1 (2013): 121-28.
9. Kim, Eunhye, and Insook Rhee Paeng. "Advantageous Sensitivity In The Dna Homolog Of The Rna Dopamine Aptamer." *Journal of Immunoassay and Immunochemistry* 35, no. 1 (2013): 83-100. doi:10.1080/15321819.2013.792833.
10. Mannironi, Cecilia, Alessia Di Nardo, Paolo Fruscoloni, and G. P. Tocchini-Valentini. "In Vitro Selection of Dopamine RNA Ligands †." *Biochemistry* 36, no. 32 (1997): 9726-734.
11. "Basal Ganglia." *SpringerReference*. doi:10.1007/springerreference\_34455.

12. Glimcher, P. W. "Understanding Dopamine and Reinforcement Learning: The Dopamine Reward Prediction Error Hypothesis." *Proceedings of the National Academy of Sciences* 108, no.
13. Supplement\_3 (2011): 15647-5654. doi:10.1073/pnas.1014269108.
14. Hegarty, Shane V., Aideen M. Sullivan, and Gerard W. O'keeffe. "Midbrain Dopaminergic Neurons: A Review of the Molecular Circuitry That Regulates Their Development." *Developmental Biology* 379, no. 2 (2013): 123-38. doi:10.1016/j.ydbio.2013.04.014.
15. Björklund, Anders, and Stephen B. Dunnett. "Dopamine Neuron Systems in the Brain: An Update." *Trends in Neurosciences* 30, no. 5 (2007): 194-202. doi:10.1016/j.tins.2007.03.006.
16. Irwin, David J., Virginia M.-Y. Lee, and John Q. Trojanowski. "Parkinson's Disease Dementia: Convergence of  $\alpha$ -synuclein, Tau and Amyloid- $\beta$  Pathologies." *Nature Reviews Neuroscience Nat Rev Neurosci* 14, no. 9 (2013): 626-36. doi:10.1038/nrn3549.
17. Editor, Business Review. "Therapy Focus: Parkinson#8217;s Disease." *PharmaDeals Review PDR* 2007, no. 80 (2007). doi:10.3833/pdr.v2007i80.390.
18. Cho, Hansang, Erh-Chia Yeh, Raghu Sinha, Ted A. Laurence, Jane P. Bearinger, and Luke P. Lee. "Single-Step Nanoplasmonic VEGF165Aptasensor for Early Cancer Diagnosis." *ACS Nano* 6, no. 9 (2012): 7607-614. doi:10.1021/nn203833d.
19. Brolo, Alexandre G. "Plasmonics for Future Biosensors." *Nature Photonics Nature Photon* 6, no. 11 (2012): 709-13. doi:10.1038/nphoton.2012.266.
20. Webb, Martin R. "Development of Fluorescent Biosensors for Probing the Function of Motor Proteins." *Mol. BioSyst. Molecular BioSystems* 3, no. 4 (2007): 249. doi:10.1039/b614154d.
21. Huang, Xiaohua, and Mostafa A. El-Sayed. "Gold Nanoparticles: Optical Properties and Implementations in Cancer Diagnosis and Photothermal Therapy." *Journal of Advanced Research* 1, no. 1 (2010): 13-28. doi:10.1016/j.jare.2010.02.002.

